AMERICAN UNIVERSITY OF BEIRUT

AN EXPERIMENTAL AND NUMERICAL ASSESSMENT OF THE BEHAVIOR OF GEOGRID-REINFORCED CONCRETE COLUMNS

by
ANAS YEHIA DAOU

A thesis
submitted in partial fulfillment of the requirements
for the degree of Master of Engineering
to the Department of Civil Engineering
of Maroun Semaan Faculty of Engineering and Architecture
at the American University of Beirut

Beirut, Lebanon
July 2018

AMERICAN UNIVERSITY OF BEIRUT

AN EXPERIMENTAL AND NUMERICAL ASSESSMENT OF THE BEHAVIOR OF GEOGRID-REINFORCED CONCRETE COLUMNS

by

ANAS YEHIA DAOU

Approved by:

Dr. Ghassan Chehab, Associate Professor — Advisor
Civil and Environmental Engineering

Dr. George Saad, Associate Professor — Advisor
Civil and Environmental Engineering

Dr. Bilal Hamad, Professor — Member of Committee
Civil and Environmental Engineering

Date of thesis/dissertation defense: July 3, 2018

AMERICAN UNIVERSITY OF BEIRUT

THESIS, DISSERTATION, PROJECT RELEASE FORM

Student Name: Yehia DAOU Anas
Last First
Middle

● Master's Thesis ○ Master's Project ○ Doctoral Dissertation

☐ I authorize the American University of Beirut to: (a) reproduce hard or electronic copies of my thesis, dissertation, or project; (b) include such copies in the archives and digital repositories of the University; and (c) make freely available such copies to third parties for research or educational purposes.

☑ I authorize the American University of Beirut, to: (a) reproduce hard or electronic copies of it; (b) include such copies in the archives and digital repositories of the University; and (c) make freely available such copies to third parties for research or educational purposes
after:

One ---- year from the date of submission of my thesis, dissertation, or project.
Two ✓ years from the date of submission of my thesis, dissertation, or project.
Three ---- years from the date of submission of my thesis, dissertation, or project.

07/16/2018

Signature Date

ACKNOWLEDGMENTS

I would like to gratefully thank my advisors Professor Ghassan Chehab and Professor George Saad for his guidance, understanding, patience and endless help throughout the past two years.

I would like to express my appreciation to Professor Bilal Hamad for participating in my thesis committee and providing me with insightful comments and helpful guidance.

Deep appreciation goes to Mr. Helmi El-Khatib for his cooperation and support. The help of the staff of the Structures and Materials lab is highly appreciated especially Abdel Rahman Sheikh. I would like to thank Mrs. Dima Al-Hassanieh for their continuous help in the lab work and for their valuable friendship.

Thanks for my colleagues at AUB for being good friends; your cheerful spirit, support, motivation and encouragement got me where I am now. Thank you for all your efforts and love.

AN ABSTRACT OF THE THESIS OF

Anas Yehia Daou for Master of Engineering
Major: Civil engineering

Title: An Experimental and Numerical Assessment of the Behavior of Geogrid-Reinforced Concrete Columns

Geogrids are geo-synthetic materials that have been established as an effective method for the strengthening of infrastructure applications and rehabilitation of slope stability problems. This study presents the results of experimental and analytical investigations on the performance of concrete columns internally wrapped with different types of Geogrids. The use of Geogrids as confinement material in the reinforced concrete columns is easier and less laborious since it is not as rigid as conventional steel reinforcement. Reinforced Concrete columns were wrapped with three different types of materials: uniaxial geogrids, biaxial geogrids, and steel hoops. The confined and unconfined (control) specimens were loaded in uniaxial compression. Strain gauges are used to qualitatively and quantitatively study the displacement and strain fields on the composite surface. Axial load and axial and lateral strains were obtained to evaluate stress-strain behavior, ultimate strength, stiffness, and ductility of the wrapped specimens. Results show that internal confinement of concrete by geogrids sheets can significantly enhance (1) the strength, (2) ductility, and (3) energy absorption capacity of the concrete specimens. An analytical model to predict the entire stress-strain relationship of concrete specimens wrapped with geogrids was developed. The finite element software package (ADINA) has been used to model reinforced concrete columns under axial stress. However, the proposed study consists of three distinct models. In the first model, the behavior is that of unconfined plain concrete. Biaxial Geogrids behavior is quantified as transverse reinforcement in the second model. In the last model, the reinforced concrete column is confined with Uniaxial Geogrids as transverse reinforcement. Comparison between the experimental and analytical results indicates that the model provides satisfactory predictions of the stress-strain response.

Keywords: Concrete; column; ductility; confined concrete; Geogrids; transverse reinforcement; confined concrete; stirrups; uniaxial geogrids; biaxial geogrids

ILLUSTRATIONS

TABLES

TABLE OF CONTENT

CHAPTER I

INTRODUCTION

A. BACKGROUND

Numerous columns within the vast infrastructure stock have been damaged due to environmental causes like corrosion. Poorly confined columns are vulnerable to dynamic loads such as those imposed by earthquakes or impacts. Failure of such columns can lead to catastrophic collapse of a building.

It has been known that lateral concrete confinement is used to delay the failure of concrete and improve its ductility. It is a feature that is critically important for structures subjected to extreme loads. This method has started with the use of synthetic fibers (FRP) (Lam & Teng, 2003) as an external confining material and steel stirrups as internal confining material. Steel stirrups have been utilized to provide lateral confinement and to strengthen deteriorated columns. An important wage of experimental and analytical studies has been conducted to investigate the behavior of concrete under numerous confining materials.

Over the last three decades, a significant number of studies has been carried out on the use of fiber reinforced polymer (FRP) composites in the construction of civil infrastructure. One popular application is the use of FRP sheets for the confinement of concrete columns. Research investigation showed that FRP sheets can enhance both strength and ductility of concrete columns by providing confinement to the concrete under concentric and eccentric compressive loadings. In addition to FRP sheets, Geogrids have been recently investigated to provide confinement to concrete. The Geogrids can be easily formed into a circular shape without sharp bends and hence the tensile capacity of the Geogrids can be used effectively. The Geogrids can also be easily

embedded into the concrete prior to casting. The thickness of concrete cover can be reduced due to the corrosion resistance property of Geogrids.

The current research work deals with the behavior of Geogrid-confined circular concrete columns subjected to concentric monotonic axial compression, aiming at developing rational constitutive models. The major objective of this project is to evaluate and quantify the effectiveness of using geogrids in Portland Cement Concrete (PCC) columns to evaluate the axial strength of confined concrete.

B. OBJECTIVE

The main objective of the proposed investigation is to evaluate the axial stress-strain response and axial load capacity of Geogrids-confined circular column sections. Several design and strength parameters are evaluated to quantify their effect on the behavior. These include the Height-to depth ratio of the column sections, the number of layers of internal Geogrids confinement, and the type of internal transverse reinforcement.

Concrete confinement increases both the ultimate strength and ductility of structural elements. Geogrids are known to possess favorable characteristics in terms of strength, ductility and ease of installation. The course of this study will provide a better understanding of the mechanisms behind the confining performance and important factors influencing it. Behavioral aspects of geogrid-reinforced concrete columns to be evaluated include maximum axial load capacity, load-deflection response, accumulated energy absorption, and modes of failure.

C. PROBLEM STATEMENT

The proposed research is significant as it allows better understanding of the effect of Geogrids confinement on the axial strength and the stress-strain response of

circular column sections. The development of a stress-strain model is extremely useful for predicting the ultimate axial capacity of Geogrids-confined columns and for conducting analytical studies of the effect of Geogrids confinement on the structural response of concrete members under different types of load applications.

The research program consists of experimental and analytical investigations, and includes the following scope:

- Review of previous research on column confinement under simulated monotonic and cyclic loading.
- Design and assembly of an experimental set-up suitable for testing full scale columns under constant axial compression and incrementally increasing lateral deformation reversals.
- Design, construction and instrumentation of fourteen full-scale circular columns with conventional longitudinal reinforcement and Geogrids Sheets as transverse reinforcement.
- Testing of fourteen columns under combined axial compression and incrementally increasing lateral deformation reversals, while recording the relevant test data by means of data acquisition systems.
- Evaluation of test data and investigation of the effects of test parameters that consist of: confining material, number of Geogrids layers, and column height.
- Development of numerical models for stress-strain relationships for concrete with Geogrids Sheets, as well as core concrete confine.
- Preparation of thesis and presentation of results.

D. ORGANIZATION OF THESIS

This thesis is organized into five chapters. Chapter 2 provides a literature review of the topic, describing the problems related with the use of PCC columns confinement; it also presents a review on the use of geosynthetics in various fields of civil engineering. The test results that include data on the general behavior and mode of failure, effect of Geogrids applications, section aspect ratio, internal reinforcement and axial stress vs. lateral strain of the specimens are presented in Chapter 4 and 5. Chapter 4 provides an introduction, description, results and analysis of the compression tests which assess the use of Biaxial Geogrids in concrete member subjected to concentric loading. The sixth and final chapter presents the summary of the major conclusions and recommendations for further research in this area.

CHAPTER II

BACKGROUND AND LITERATURE REVIEW

A. INTRODUCTION

One of the design capacity principles is to ensure that reinforced concrete (RC) buildings exhibit a ductile behavior with the help of stirrups under the impact of earthquakes. For this purpose, a number of experimental studies have been conducted to investigate the effects of steel (Michels, Waldmann, Maas, & Zürbes, 2012) & (Y. Park, Abolmaali, Mohammadagha, & Lee, 2015) and plastic fibers (Pujadas, Blanco, Cavalaro, & Aguado, 2014) & (Lee & Won, 2014) on the flexural and shear strength of RC members. New materials are also being investigated by the construction industry. These materials have characteristics such as increased ductility and low weight to reduce inertial forces as well as reduce cost. The geo-grid is a geo-synthetic material that has been widely used in research studies. Different studies have been performed to obtain new solutions for the construction industry, which has shown increasing interest in geo-grids. While many studies have been performed on geo-grids for asphalt(Khodaii, Fallah, & Moghadas Nejad, 2009; Liu & Ling, 2001), retaining walls, foundations(Demir, Yildiz, Laman, & Ornek, 2014; Yetimoglu, Wu, & Saglamer, 1994), pavements (Article Scientific research & essays · November 2010, ; Norambuena-Contreras & Gonzalez-Torre, 2015), and airports (Abdesssemed, Kenai, & Bali, 2015a), only a few studies have used geo-grids as alternative transverse reinforcement bars in RC members(Yalciner, Kumbasaroglu, Ertuc, & Turan, 2018).

It has been known that lateral concrete confinement is used to delay the failure of concrete and improve its ductility. It is a feature that is critically important for structures subjected to extreme loads. This method has started with the use of synthetic

fibers (FRP) as an external confining material and steel stirrups as internal confining material. Steel stirrups have been utilized to provide lateral confinement and to strengthen deteriorated columns. An important wage of experimental and analytical studies has been conducted to investigate the behavior of concrete under numerous confining materials.

Over the last three decades, a significant number of studies have been carried out on the use of fiber reinforced polymer (FRP) (Lam & Teng, 2003) composites in the construction of civil infrastructure. One popular application is the use of FRP sheet for the confinement of concrete columns. Research investigation showed that FRP sheet can enhance both strength and ductility of concrete columns by providing confinement to the concrete under concentric and eccentric compressive loadings. In addition to FRP sheet, Geogrids has been recently investigated to provide confinement to concrete. The Geogrids can be easily formed into a circular shape without sharp bends and hence the tensile capacity of the Geogrids can be used effectively. The Geogrids can also be easily embedded into the concrete prior to casting. The thickness of concrete cover can be reduced due to the corrosion resistance property of Geogrids.

The current research work deals with the behavior of Geogrid-confined circular concrete columns subjected to concentric monotonic axial compression, aiming at developing rational constitutive models. The major objective of this project is to evaluate and quantify the effectiveness of using geogrids in Portland Cement Concrete (PCC) columns to evaluate the axial strength of confined concrete.

B. LITERATURE REVIEW

1. Geogrid Polymers: Definition, Usage, Classification and Advantages

Geogrids belong to the family of geosynthetic materials made from polymers such as polypropylene, polyethylene or polyester. They are commonly used for soil stability purposes in road embankments (Abdesssemed, Kenai, & Bali, 2015b) (Maxwell, et al. 2005) or reinforced earth walls due to their tensile reinforcing capability (Palmeira, et al. 2008).

Geogrids are commonly classified as uniaxial, biaxial, or triaxial based on the number of directions they reinforce. Each of these types could either be woven or punched-drawn non-woven based on their physical properties, mechanical properties, and manufacturing process.

The use of geogrids in concrete is not as common as their use in soils. However, increasing efforts are recently being invested to assess the feasibility of using geogrids to reinforce Portland cement concrete (PCC) in order to benefit from their tensile strength and ductility. The results from most studies were very promising in that regard, as concrete gained both post-cracking ductility and load capacity. The developed Finite Element (FE) models can help predict the behavior of geogrid-reinforced concrete applications for various conditions and configurations not studied experimentally.

2. Previous applications on geogrids use in concrete

Itani et al. (Itani, Saad, & Chehab, 2016) introduced geogrids in thin concrete overlays to study its effectiveness in preventing reflective cracking as well as providing concrete with post-cracking ductility. Uniaxial geogrids of high tensile strength were used in this study. Two experimental setups were adopted to achieve the desired objectives.

On one side, the direct tension test was conducted to simulate thermal loads. Control specimens, formed with plain concrete, exhibited brittle failure as they split in half, while geogrid reinforced concrete specimens showed an increase in strength after initial cracking of concrete. This can be explained by the fact that the geogrid continues to resist loading after the failure of concrete. Thus, it was concluded that geogrids provide concrete with post cracking ductility (Itani et al., 2016). In addition, it was found that geogrid reinforced concrete can withstand a higher load than plain concrete.

On the other side, traffic loads were approached using the flexural test with both monotonic and cyclic loading. The results of the monotonic loading test showed that the geogrid reinforced concrete samples cracked earlier than the plain concrete ones. The authors related this behavior to the fact that the geogrid layer is splitting the concrete sample into two parts acting separately and thus weakening the section (Itani et al., 2016). During the post-cracking phase, the plain concrete specimens split in half as the crack propagated all the way to the upper surface of the slab while for the geogrid reinforced concrete specimens, the crack was arrested by the geogrid sheet which continued to resist the load after the failure of concrete. The same results were found for the cyclic loading test in the pre-cracking and post-cracking phases.

Al Ayyash et al. conducted an experimental study to assess the advantages of using geogrids as a confinement tool in Portland Cement Concrete cylinders taking into consideration different types of geogrids (uniaxial and biaxial) and different number of reinforcement layers (one layer and two layers). It should be noted that the tensile strength of the biaxial geogrids is lower than that of the uniaxial ones. Plain concrete cylinders exhibited brittle failure. Cylinders confined with 2 layers of uniaxial geogrid hoops showed the highest ductility after initial cracking of concrete. However, cylinders confined with 2 layers of biaxial geogrids were not tested. Cylinders confined with 1

layer of uniaxial geogrid, and those confined with 1 layer of biaxial geogrid showed a similar behavior in the post-cracking phase to cylinders confined with steel hoops.. In addition, it was found that the cylinder confined with 1 layer of biaxial geogrid had the highest ultimate axial load which indicates that the mesh shape of the biaxial geogrid, which resulted in a better confinement effect, is the factor that resulted in additional compressive strength rather than the geogrid's tensile strength noting that the tensile strength of biaxial geogrids is relatively lower than that of the uniaxial type.

El Meski and Chehab (Chehab & El Meski, 2014) used uniaxial, biaxial, and triaxial geogrids with different physical and mechanical properties to reinforce nine normal strength and six high strength concrete beams. The specimens were then subjected to four-point monotonic load bending until failure. Comparing the load-deflection results of geogrid-reinforced beams to those of plain concrete ones, a much larger deflection was observed for all geogrid-reinforced samples indicating a very ductile post-cracking behavior compared to a brittle failure in the plain concrete specimens. In addition, it was found that until the initial crack occurred, only concrete was resisting the load (Chehab & El Meski, 2014). This was evident by observing the same pre-cracking behavior for all types of geogrids. The initial crack appeared earlier for geogrid-reinforced members due to the weaker concrete section separated by the geogrid sheet. However, in the post-cracking stage, the CMOD increases gradually as the geogrids resist the load until they fail. Finally, the flexural strength increased by 20%, 12%, and 28% when using uniaxial, biaxial, and triaxial geogrids respectively with normal strength concrete, noting that the increase was much lower for high strength concrete (Chehab & El Meski, 2014).

Tang et al. (X. Tang, G.R. Chehab, & S. Kim, 2008) also investigated the behavior of geogrid-reinforced PCC members by comparing the effect of introducing

one or two layers of stiff and flexible biaxial geogrids. Similar benefits of using geogrid reinforcement were observed in terms of improved post-cracking ductility, load capacity, and energy absorption capacity. Stiff geogrids were found to achieve better overall results compared to flexible geogrids which implies that the physical and mechanical properties of the geogrids are a key factor in the efficiency of concrete reinforcement. Finally, introducing a second geogrid layer caused a significant increase in post-cracking ductility and load capacity which peaked at approximately 60% of the maximum load that caused the first crack (X. Tang et al., 2008).

Sivakamasundari et al. (Sivakamasundari, Daniel, & Kumar, 2017) investigated the effectiveness of using biaxial geogrids as shear reinforcement along with steel fibers. On one side, compressive and tensile behavior of three types of specimens were compared: a control cylinder made of plain concrete, another one confined with a tubular shaped biaxial geogrid and a third one similar to the second but adding steel fibers. Testing results showed that the use of geogrid confinement with steel fibers increased both compressive and tensile strength of the specimens (Sivakamasundari et al., 2017). On the other side, concrete beams, with different shear reinforcement techniques, were casted and tested under three-point monotonic loading. A control beam transversally reinforced with steel stirrups only, another beam containing, in addition to the previous, biaxial geogrid-transverse reinforcement in hinge region, and a third one with a certain amount of steel fibers along with steel stirrups and geogrids. It was concluded that the use of geogrid-transverse reinforcement along with steel fibers resulted in a significant improvement of the post cracking behavior as well as energy dissipation capacity of the beams compared with the use of geogrids alone.

Al Hedad et al. (Al-Hedad, Bambridge, & Hadi, 2017) studied the effect of using geogrids on the drying shrinkage behavior of concrete pavements. To achieve the stated objective, two types of specimens were prepared, cured for 7 days according to two different stages and then placed in a drying chamber until 56 days from casting the specimens. The first type consisted of concrete prisms, of 75 mm thickness, among which some specimens were control and others contained one sheet of biaxial geogrid placed at one of two different locations from the top (20 mm or 37.5 mm). Testing results of these specimens showed that after 14 days from casting the specimens, geogrid reinforcements were able to reduce the drying shrinkage strains by 0.7 – 15% compared with the unreinforced prisms (Al-Hedad et al., 2017). However, geogrid sheets placed at 20 mm from the top were more effective during the early stage than those placed at 37.5 mm in terms of reducing drying shrinkage strains. After 21 days, both groups (placed at 20 mm and 37.5 mm) had approximately the same effect. The second type included concrete slabs, of 30 mm thickness, among which some specimens were plain concrete and the others reinforced with one sheet of biaxial geogrid placed at 15 mm from the top. It was noticed that drying shrinkage strains were reduced by 7-28% compared to plain concrete slabs (Al-Hedad et al., 2017).

Chidambaram and Agarwal (Chidambaram & Agarwal, 2016) tested beam-column joint specimens under cyclic loading with and without geogrid confinement. Results showed that geogrid confinement at the joint resulted in an improved performance in terms of strength, stiffness and damage index (Chidambaram & Agarwal, 2016).

In another study, the authors (Siva Chidambaram & Agarwal, 2015) used geogrids for shear reinforcement in steel-reinforced concrete beams. Specimens were tested under single point monotonic loading. Testing results showed that geogrid shear

reinforcement significantly enhanced the post-cracking behavior of the beams (Siva Chidambaram & Agarwal, 2015).

Chidambaram and Agarwal (Siva Chidambaram & Agarwal, 2014) also tested the effectiveness of confining concrete specimens with geogrids under compressive, flexural and tensile loading. It was concluded that the use of geogrids as a confinement mechanism for concrete resulted in a significant improvement in the behavior of concrete compared with conventional confinement techniques (Siva Chidambaram & Agarwal, 2014). Furthermore, it was found that the number of layers of geogrids used for confinement as well as their mechanical properties had a major effect on the load-deformation behavior of concrete (Siva Chidambaram & Agarwal, 2014).

3. Fracture mechanics

Fracture modes were presented in the report done by (Mander, Priestley, & Park, 1988) based on the work of Elwi and Murray (1979));

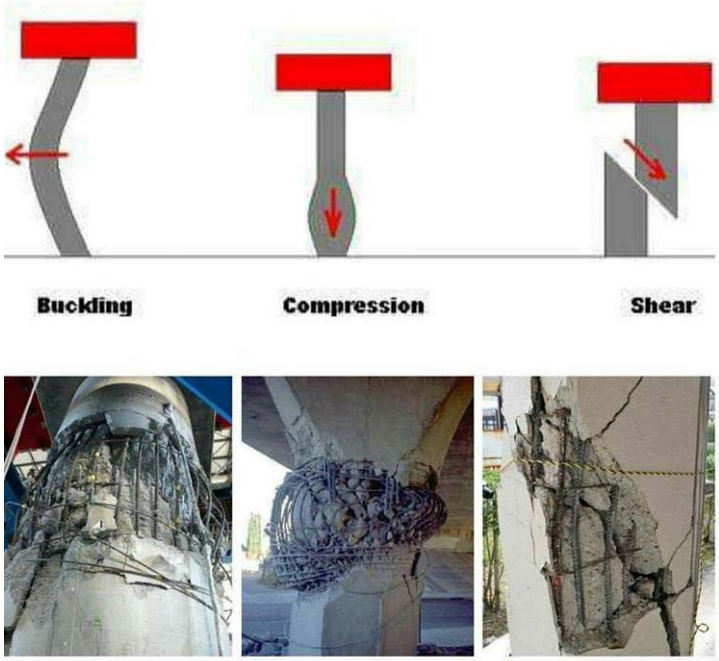

Figure 1 Circular RC Column Failure

Based on the slenderness ratio of the column, there are three modes of failure of reinforced concrete columns. The columns are assumed to be centrally loaded (no eccentric loads). (Figure 1)

Mode – 1: Column Failure due to Pure Compression

Mode – 2: Column Failure due to Combined Compression and Buckling

Mode – 3: Column Failure due to shear

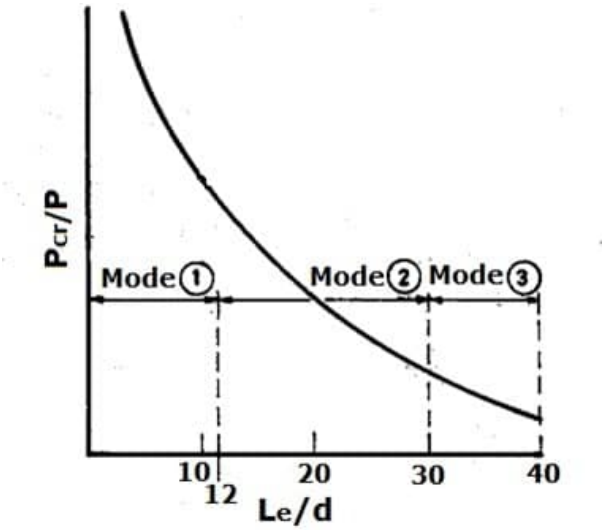

Figure 2 Failure Modes of Concrete Columns for Different Slenderness Ratio

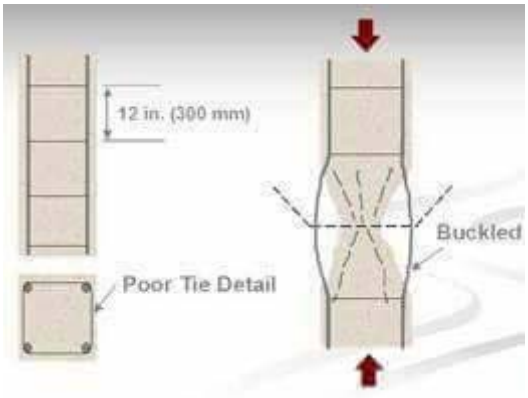

Figure 3 Buckling of steel reinforcement

4. Previous research on confinement of concrete columns

Numerous experimental and analytical studies have been conducted recently to evaluate the axial strength and stress-strain response of concrete confined with Different Confining material, especially FRP jackets as external confining material and Steel

stirrups as internal confining material (ACI committee 440 on FRP composites - update.2000). These studies have clearly demonstrated that confining concrete with Steel stirrups leads to considerable enhancement of the axial strength and energy absorption capacity of concrete columns subjected to both static and cyclic loading. The same studies have also identified the following as being the main factors that influence the axial strength of PCC confined columns: the number or area of confining material wraps; the modulus of elasticity and strength of the confining material; the shape of the column section (rectangular or circular); the height-to-depth of the column section (rectangular or circular); and the aspect ratio of the column section (rectangular columns). On the other hand, several confinement models were proposed in some studies to evaluate the axial strength of columns. They describe the stress-strain response of FRP jacketed columns.

However, Teng and Lam (Lam & Teng, 2004; Teng & Lam, 2004) establish a comprehensive review and assessment of existing models. According to Teng and Lam, the proposed stress-strain models of FRP confined concrete can be classified mainly into two major categories: “design-oriented” and “analysis-oriented” models. In the design-oriented models, experimental data are evaluated to generate the stress-strain curve (Lam & Teng, 2004; Teng & Lam, 2004). This type of stress-strain relationships is simple and applied in design calculations. In the analysis-oriented models, the stress-strain curve is generated by considering interaction between the concrete core and the confining FRP.

Independent of the confining material type, the proposed stress-strain relationships are based on the confined-concrete model with hydrostatic pressure, proposed in 1929 by Richart et al. from tests conducted on concrete specimens:

$$f'_{cc} = f'_c * \left(1 + K_1 * \frac{f_l}{f'_c}\right)$$

$$\varepsilon_{cc} = \varepsilon_0 * \left(1 + K_2 * \left(\frac{f'_{cc}}{f'_c} - 1\right)\right)$$

Where f'_{cc} and ε_{cc} are the confined concrete compressive strength and corresponding strain, respectively; f'_c and ε_0 are the compressive strength and corresponding strain for unconfined concrete; K_1 is the confinement effectiveness coefficient and f'_l is the lateral hydrostatic pressure. Richart et al. (1929) found values for K_1 = 4.1 and K_2 = 5.

In the same context, the Mander et al. (Mander et al., 1988) proposed popular expressions for evaluating the effect of confinement on the axial strength of concrete steel confined columns. In the following expression, the confined concrete compression strength f'_{cc} and its strain ε_{cc}, calculated at the point of yield of transverse steel, are expressed in function of the effective lateral confining pressure f_l as follows:

$$f'_{cc} = f'_c * \left(-1.254 + 2.254 * \sqrt{1 + \frac{7.94 * f_l}{f'_c}} - 2 * \frac{f_l}{f'_c}\right)$$

$$\varepsilon_{cc} = \varepsilon_0 * \left(1 + 5 * \left(\frac{f'_{cc}}{f'_c} - 1\right)\right)$$

Lam and Teng (Lam & Teng, 2003) used a database consisting of 76 specimens confined with carbon, glass or aramid FRP existing in the literature. Based

on their analysis-oriented model, if the confinement radio $\frac{f_l}{f'_{co}}$ is larger than 0.07 an

ascending post-peak branch is expected leading to a considerable strength enhancement. For the cases of confined specimens with a confinement ratio less than 0.07 a stress-strain curve with a descending post-peak branch is expected and no considerable strength enhancement is assumed.

As design-oriented stress-strain model for FRP confined concrete was developed by number of authors, this study deals with the development of a stress-strain model for Geogrid-confined concrete model. The latest design-oriented model to describe the stress-strain response of FRP jacketed circular columns is the one proposed by Lam and Teng (2003a and 2003b). Because of its relevance to the current investigation and its simplicity in application, the model of Lam and Teng, shown below (**Figure *4***), is presented in this study for comparative purposes.

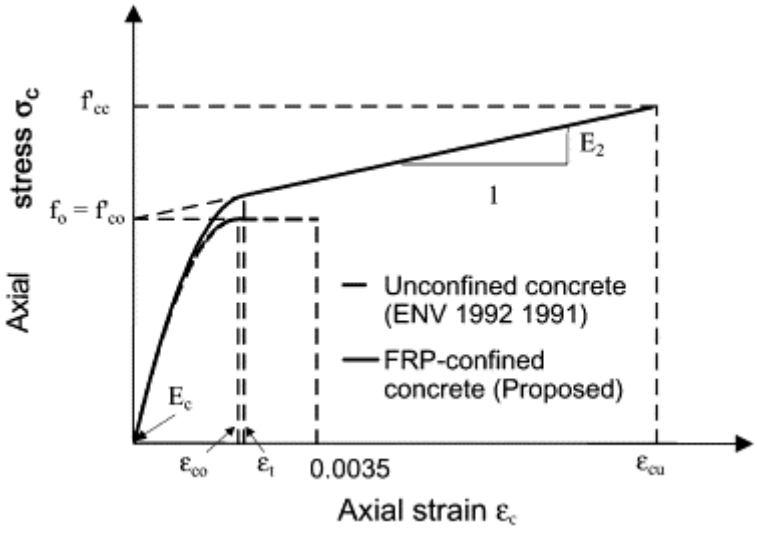

Figure 4 Stress-Strain model proposed by Lam and Teng

CHAPTER III

EXPERIMENTAL PROGRAM

A. PRELIMINARY STUDY

In order to fully understand the behavior of the Geogrids confined concrete, the tensile strength of the different types of Geogrids was investigated. The tensile testing was done using the ASTM D 3822-14 the 'Standard for Tensile Properties of Single Fibers'. Figure 5 shows direct tension test and is applied to the different types of Geogrids.

The key testing points are listed below:

Strain Gauge: the strain Gauge was used to get the strain at the fracture location in the Geogrids

Constant rate of extension: the rate of extension or pull was set 15 mm/min for all the fiber tests.

Clamps: clamps with flat jaws were used to grip the fiber specimens and minimize their slippage

For the analytical part of this study, nonlinear finite element models were built using the Automatic Dynamic Incremental Nonlinear Analysis "ADINA". It is a commercial package which was founded in 1986 by Dr. Klaus-Jürgen Bathe. ADINA-AUI 9.0.1 is the version used for the analysis.

1. Material Characterization: Geogrids

A direct tension test is applied to the different types of Geogrids, to get its stress strain curve (Figure 6 and Figure 7). This will be used in defining the behavior of the geogrids in the analytical model.

Figure 5 Direct tension test on (a) Uniaxial Geogrid (b) Biaxial Geogrid

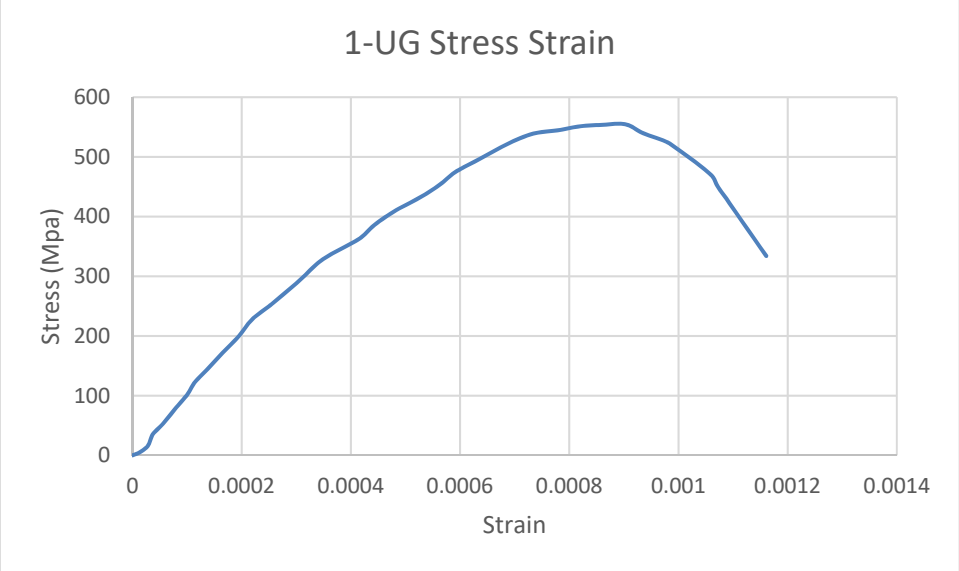

Figure 6 Stress-strain curve of the uniaxial Geogrids

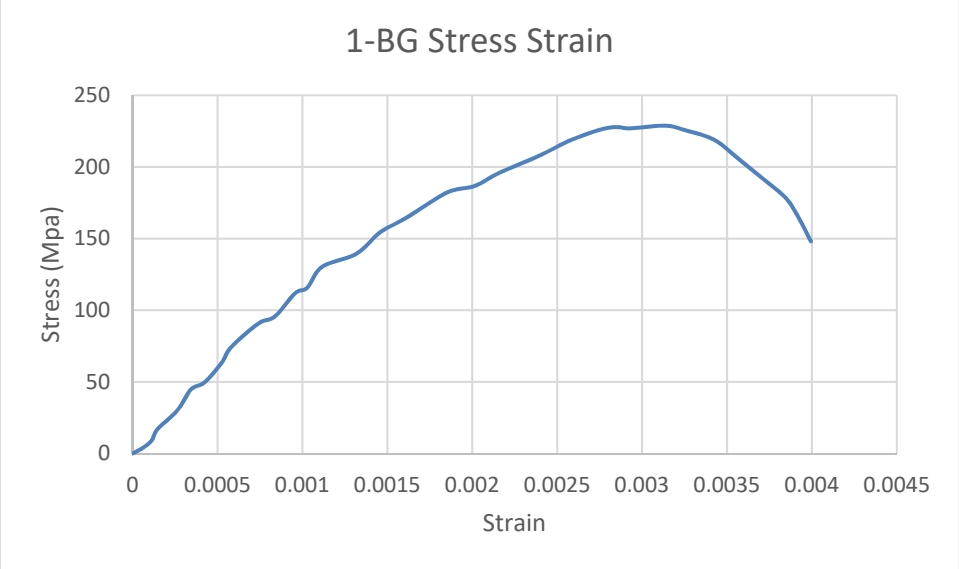

Figure 7 Stress-strain curve of the biaxial Geogrids

2. *Material Characterization: Concrete*

A compressive test is applied to a typical concrete cylinder. Figure 8 shows the stress strain behavior of a typical concrete cylinder test, used to determine the concrete compressive strength. The analytical model was validated, and results were compared with this test results.

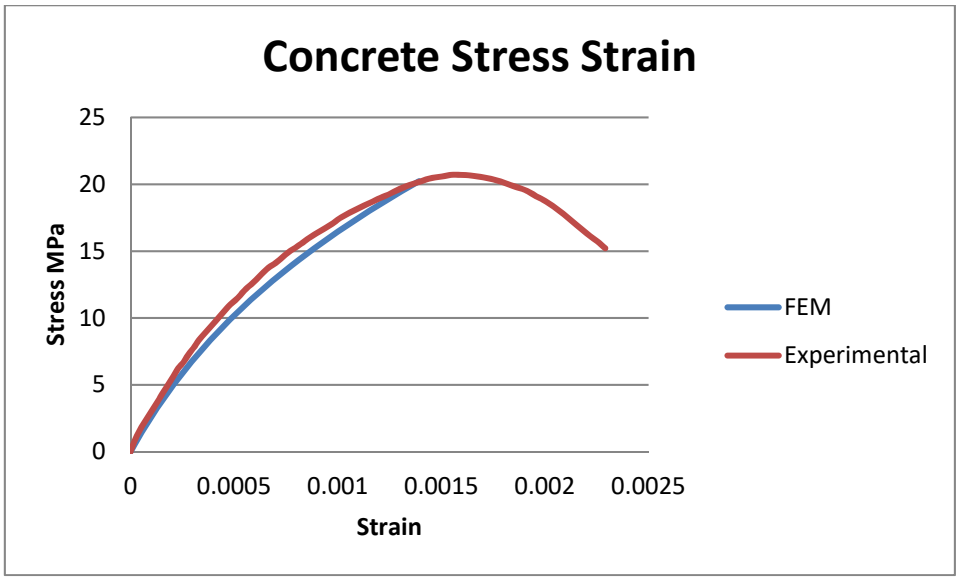

Figure 8 Plain Concrete Stress Strain

The 25x50 cm specimens were discretized in three dimensions. Three 3-dimensional models were created, the first one is the plain concrete model (Figure 9), the second is the Uniaxial Geogrids reinforced model (Figure 10), and the third is the Biaxial Geogrids reinforced model (Figure 11 & Figure 12).

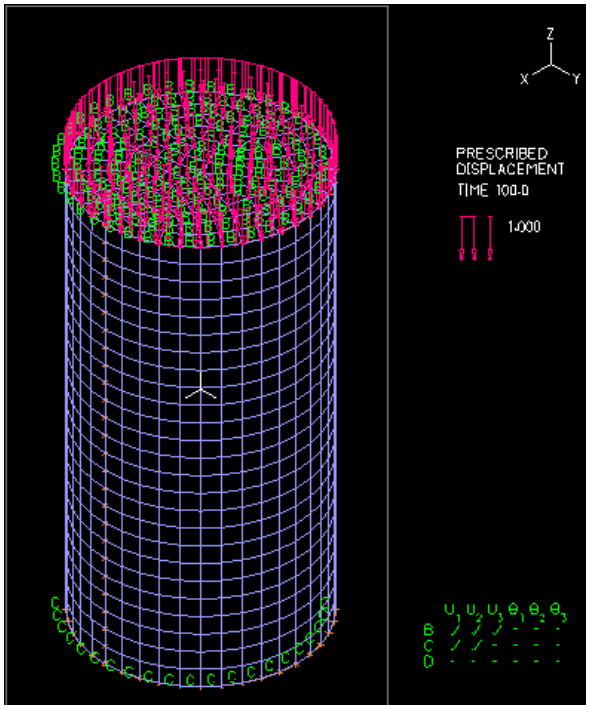

Figure 9 Plain concrete 3D-model column

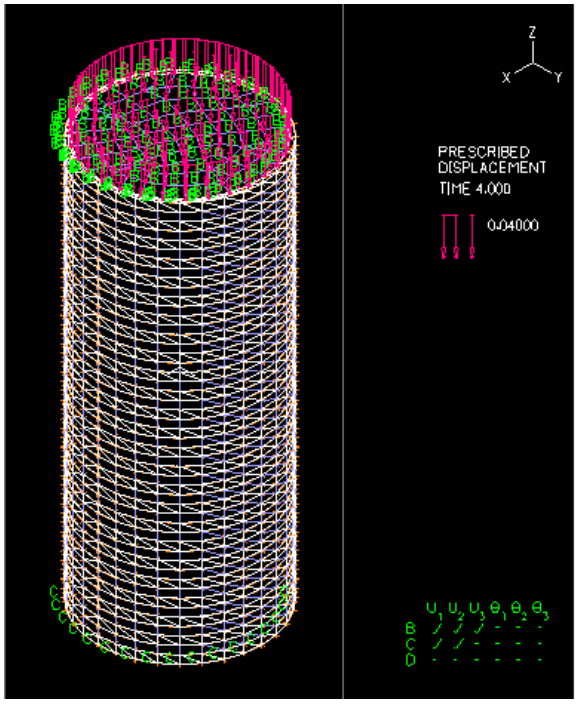

Figure 10 Geogrid reinforced concrete 3D-model showing the ribs of the Uniaxial geogrids

An incremental solution process was used using the full Newton method and line searches criteria. The lower surface of the column is fixed against all degrees rotational of freedom and the upper surface is subjected to a uniform displacement in

the Z-direction. The magnitude of the prescribed displacement was set such that the model will fail at the chosen value.

The FEM mesh consists of three dimensional solid elements with 10 nodes each. The constitutive material model for concrete is the concrete model found in ADINA's material library. It is a nonlinear, multi-axial constitutive model which has the characteristic of failing in tension at a maximum, relatively small, tensile stress and a crushing failure due to high compression (ADINA 2012). As for the geogrid material, the stress-strain curve was obtained by apply direct tension test to the geogrid and it was defined as "Multilinear Elastic-plastic material" in ADINA.

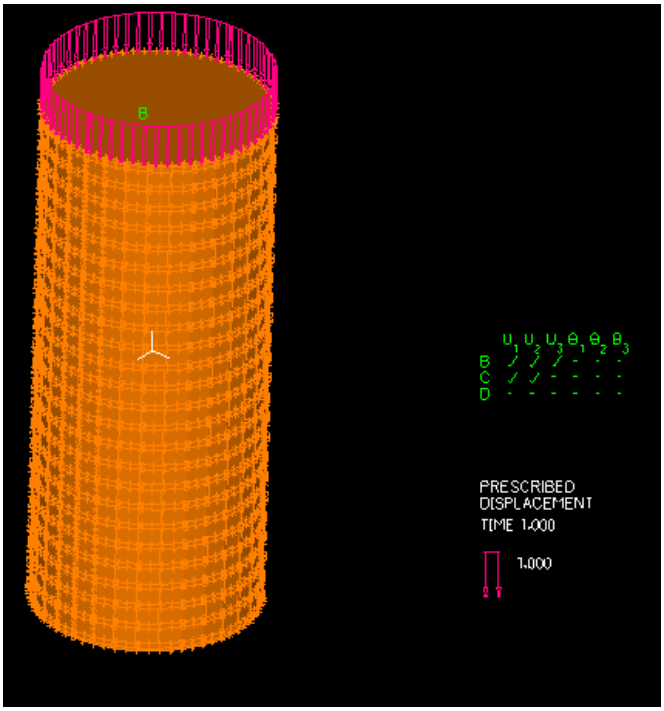

Figure 11 Geogrid reinforced concrete 3D-model showing the ribs of the Biaxial geogrids

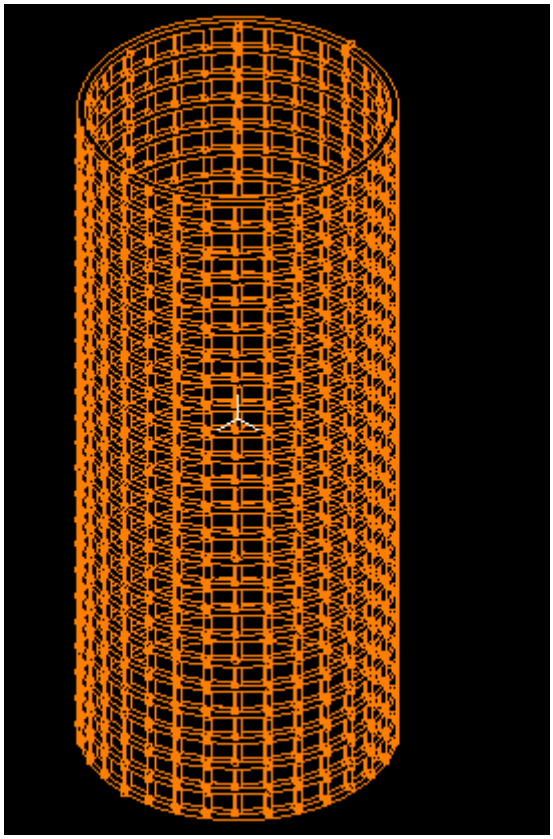

Figure 12 Biaxial Geogrid Model

3. Preliminary results

Three models were created to stu the crack propagation (Figure 13 & Figure 14).

It is noticeable from the Stress Strain curves that the geogrid improves the concrete response to the load by increasing the strength in compression. The results presented in Figure 13 and Figure 14 clearly indicate that the use of Geogrids confinement leads to significant increases of the axial stress capacity of circular columns.

As a result of these combined advantages of the Geogrids confinement, the increases of axial strength for the Geogrids Confined R/C column specimens were considerably larger in comparison with their companion plain concrete specimens for all

column aspect ratios. For instance, using one Geogrids layer increases the axial capacity of the reinforced concrete column specimens by 56 %, and 65% for the specimens.

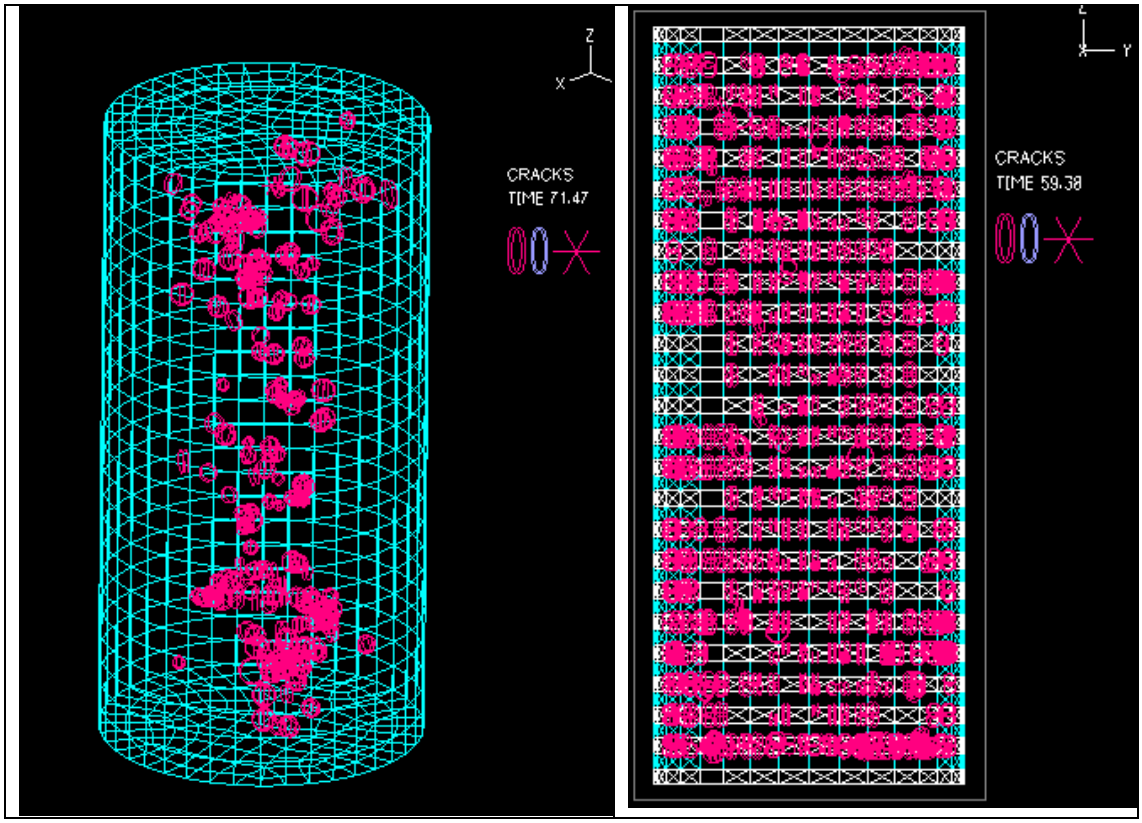

Figure 13 Concrete Column model cracks pattern (a) Plain (b) Uniaxial Geogrid reinforced

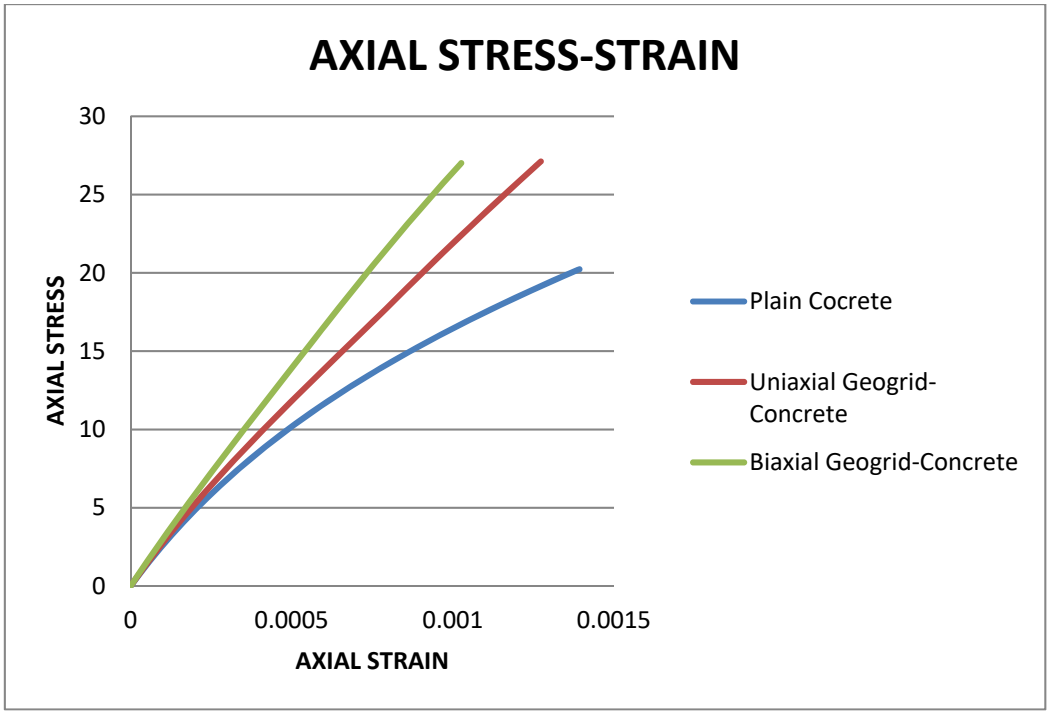

Figure 14 Stress strain curve

It is noticeable from the lateral Stress Strain curves (Figure 15 & Figure 16) that the geogrid improves the concrete response by increasing the lateral capacity, whereas in the plain concrete column response, the lateral stress tends to be negligible.

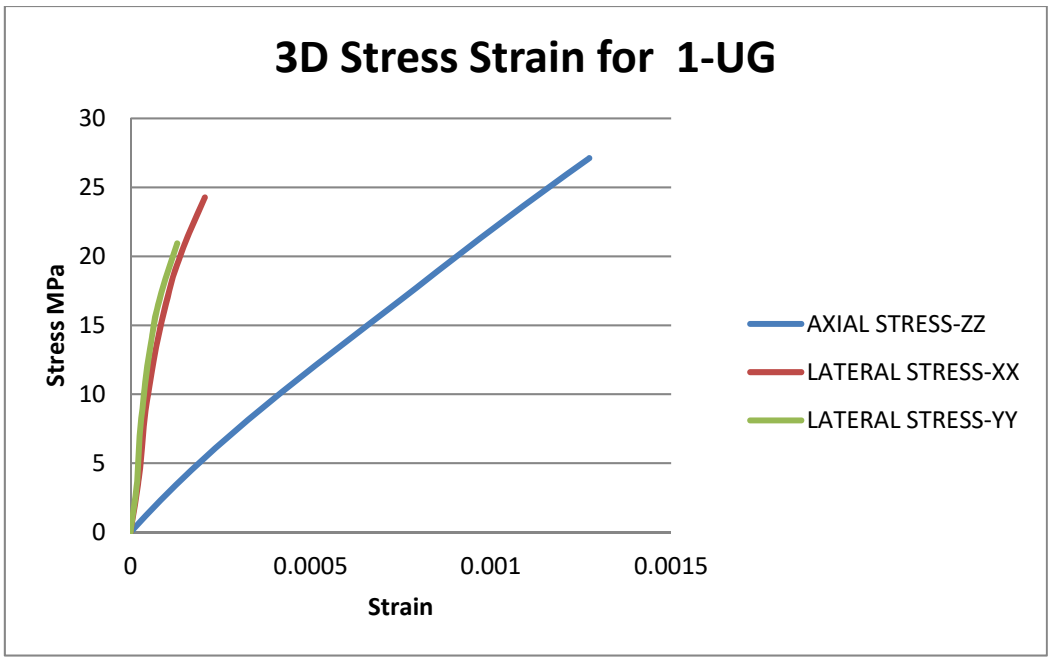

Figure 15 Stress strain curve of Uniaxial Reinforced Concrete Column

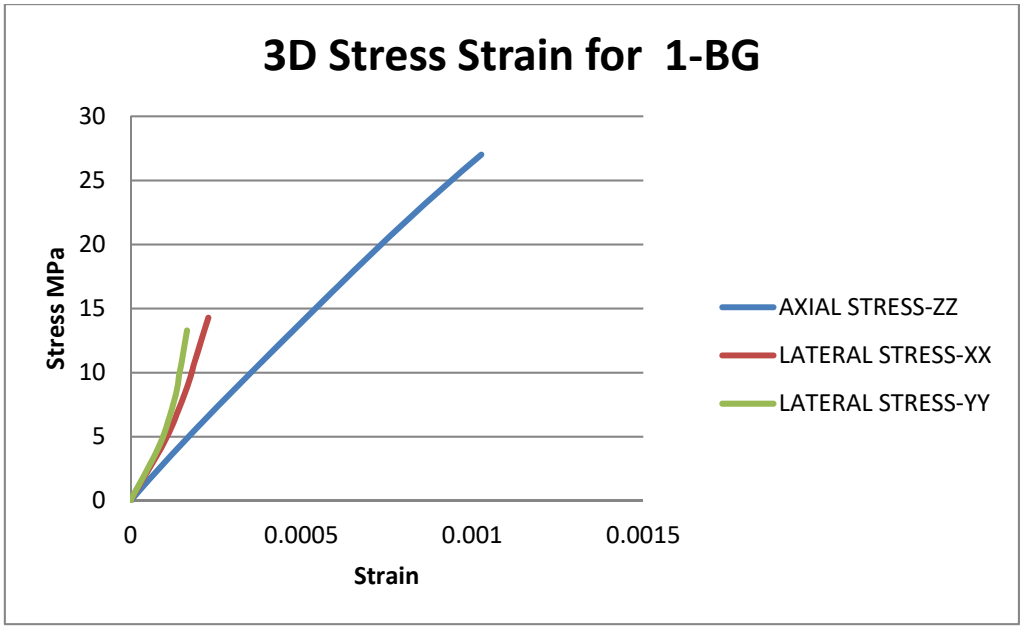

Figure 16 Stress strain curve of Biaxial Reinforced Concrete Column

The stress-strain response of Geogrids confined circular concrete column sections was analytically investigated.

The following conclusions and observations can be drawn from this study:

1. Confining circular columns with Geogrids leads to substantial improvement in the axial strength of compression failure of the columns.
2. The calibrated Geogrids material can be used to predict the effect on introducing geogrids in circular concrete column.
3. The stress-strain response of Geogrids confined columns experiences a considerable decrease in lateral strain, and consequently a distinct change in behavior, beyond a confined lateral strain of about 2000 Macrostrains.

B. TEST SPECIMENS AND TEST PARAMETERS

Twenty eight small-scale column specimens of variable height with fourteen replicates are prepared for testing under axial monotonic compression loading.

Replicates are used to validate the experimental test results. The main test variables include confining material, number of Geogrids layers, and the height to diameter ratio or the aspect ratio D/L of the section. Two types of Geogrids confinement and four different aspect ratios are evaluated. For each set of variables, two column specimens are prepared for testing. The specimens are divided into four series (P, S, BG, and UG) depending on their confining material shape. The terms P and S represent column with no confining material and with steel hoops as confining material, respectively, while BG and UG represent Biaxial Geogrids and Uniaxial Geogrids as confining material, respectively. Table 1 provides a summary of the specimens' designations, sizes and corresponding test parameters. While the aspect ratios D/L of the column sections in all test series are different, the areas of all sections are almost identical. The number following UG and BG corresponds to the column height, while the number following S corresponds to the steel hoop spacing.

Table 1 Test variables

	Geometry					Material			
Specimen	D (mm)	L (mm)	D/L	r (mm)	Slenderness Ratio KL/r	f'cu (Mpa)	Type of Reinforcement	Spacing (mm)	Number of layers
P(1)	230	500	0.46	57.50	21.74	11	none	-	-
P(2)	230	500	0.46	57.50	21.74	11	none	-	-
BG-50-1L(1)	230	500	0.46	57.50	21.74	11	biaxial Geogrids	-	1
BG-50-1L(2)	230	500	0.46	57.50	21.74	11	biaxial Geogrids	-	1
BG-50-2L(1)	230	500	0.46	57.50	21.74	11	biaxial Geogrids	-	2
BG-50-2L(2)	230	500	0.46	57.50	21.74	11	biaxial Geogrids	-	2

UG-50-1L(1)	230	500	0.46	57.50	21.74	11	Uniaxial Geogrids	-	1
UG-50-1L(2)	230	500	0.46	57.50	21.74	11	Uniaxial Geogrids	-	1
UG-50-2L(1)	230	500	0.46	57.50	21.74	11	Uniaxial Geogrids	-	2
UG-50-2L(2)	230	500	0.46	57.50	21.74	11	Uniaxial Geogrids	-	2
S5(1)	230	500	0.46	57.50	21.74	11	stirrups	50	-
S5(2)	230	500	0.46	57.50	21.74	11	stirrups	50	-
S10(1)	230	500	0.46	57.50	21.74	11	stirrups	100	-
S10(2)	230	500	0.46	57.50	21.74	11	stirrups	100	-
S15(1)	230	500	0.46	57.50	21.74	11	stirrups	150	-
S15(2)	230	500	0.46	57.50	21.74	11	stirrups	150	-
S20(1)	230	500	0.46	57.50	21.74	11	stirrups	200	-
S20(2)	230	500	0.46	57.50	21.74	11	stirrups	200	-
BG-40-1L	230	400	0.58	57.50	17.39	11	biaxial Geogrids	-	1
BG-45-1L	230	450	0.51	57.50	19.57	11	biaxial Geogrids	-	1
BG-55-1L	230	550	0.42	57.50	23.91	11	biaxial Geogrids	-	1
BG-60-1L	230	600	0.38	57.50	26.09	11	biaxial Geogrids	-	1
UG-40-1L	230	400	0.58	57.50	17.39	11	Uniaxial Geogrids	-	1
UG-45-1L	230	450	0.51	57.50	19.57	11	Uniaxial Geogrids	-	1
UG-55-1L	230	550	0.42	57.50	23.91	11	Uniaxial Geogrids	-	1
UG-60-1L	230	600	0.38	57.50	26.09	11	Uniaxial Geogrids	-	1

C. MATERIALS AND SPECIMENS PREPARATION

1. Concrete Material

All specimens were cast using a single batch of Ready Mix concrete (Zoughaib, Beirut, Lebanon). The concrete material to be used consists of Portland cement Type I, sand, and well graded coarse aggregate having 9.5 mm maximum size. Because of the limited capacity of the axial testing machine, the water-cement ratio will be calibrated to produce concrete compressive strengths of about 11 MPa. Standard 150 x 300 mm cylinders are cast and tested to check the concrete compressive strength. The specimens were prepared to cast in one batch, corresponding to all the plain concrete specimens, and for all internally reinforced ones.

2. Geogrids

The physical and mechanical properties of geogrids are a major factor of the confining effectiveness for concrete; Tang et al. (X. Tang et al., 2008) noted that the difference in the performance of different geogrids for the same concrete mixture is due to difference in their physical and mechanical properties. The geogrid to be used is considered stiff geogrid and made of high density polyethylene.

Uniaxial geogrids consist of one-directional thin ribs joined together at thicker junctions; hence, they provide tensile reinforcement in the longitudinal direction of the ribs. Physical and mechanical properties of uniaxial geogrids as obtained from the manufacturer (TENAX 2003) are presented in **Error! Reference source not found.**.

Biaxial geogrids consist of two-directional thin ribs joined together at thicker junctions; hence, they provide tensile reinforcement in both longitudinal and transverse directions. The geogrids used for this study are punched-drawn non-woven stiff

geogrids made up of polypropylene. Their physical and mechanical properties, as obtained from the manufacturer, are presented in **Error! Reference source not found.**.

Figure 1 and 19 show the different forms of the geogrids used as reinforcement. In order to from the required cylindrical shape, a wide geogrid sheet is carefully rolled and fixed into place with sufficient overlap. As these are stiff geogrids, the minimum diameter that could be achieved is 15 cm.

The geogrids sheets were applied in the transverse direction around the columns with 300 mm overlap for both one and two layered specimens.

Table 2- Physical and mechanical properties of the uniaxial geogrids

Component	Description	Unit
Aperture size MD	220	mm
Aperture size TD	13/20	mm
Mass per unit area	400	g/m2
Strength at 2% strain	17	kN/m
Strength at 5% strain	32	kN/m
Peak tensile strength	160	kN/m
Yield point elongation	13	%
Junction strength	50	kN/m
Long term design strength	28.3	kN/m

Table 3: Physical and Mechanical Properties of the Biaxial Geogrids

Property	Unit	Value
Load at 2% strain	kN/m	14
Load at 5% strain	kN/m	28
Ultimate Tensile Strength (L/T)	kN/m	40/40
Strain at Tult (L/T)	kN/m	11/10
Opening size (L/T)	mm	33/33
Rib width (L/T)	mm	2.2/2.5
Rib thickness (L/T)	mm	2.2/1.4
Junction thickness	mm	5.8

Note : L = Longitudinal direction ; T = Transverse direction

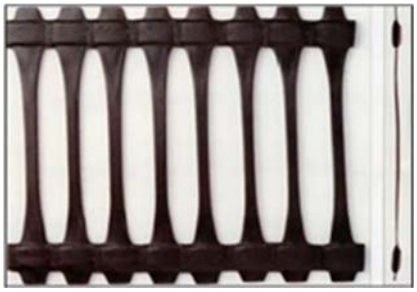

Figure 17 View of Uniaxial geogrid layer

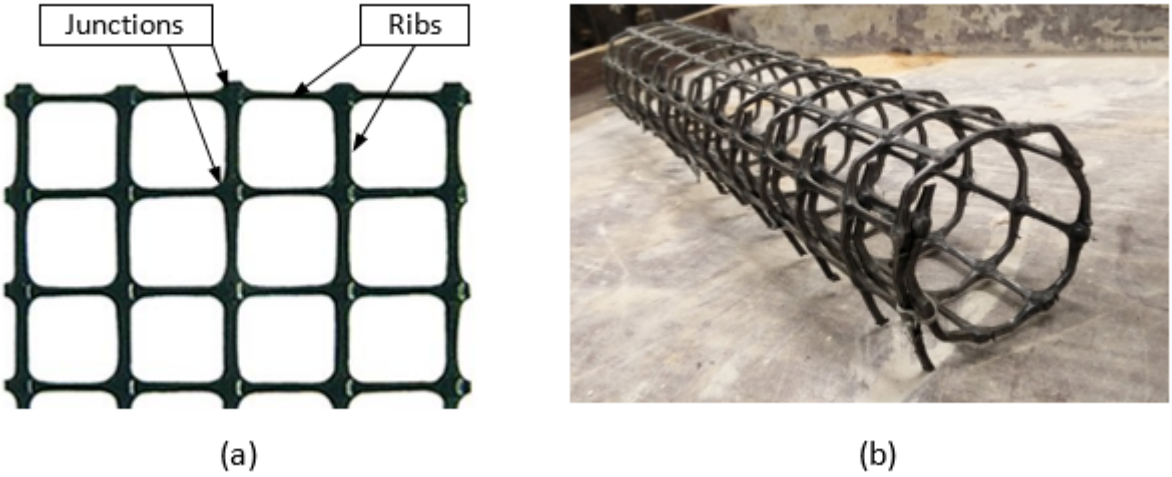

Figure 18 View of Biaxial geogrid geometry for (a) geogrid layer and (b) geogrid cylindrical member

3. Mixing and Casting

All specimens were cast using a single batch of Ready Mix concrete (Zoughaib, Beirut, Lebanon). The concrete mix consisted of coarse aggregate having 9.8 mm maximum size, natural sand, and Portland cement (Type I). The 28-day concrete compressive strength, obtained using standard 15 × 30 cm concrete cylinders, was measured at 11 MPa for all specimens.

4. Reinforcing Steel

The steel reinforcement in the reinforced concrete column specimens consists of four 10 mm Grade 60 deformed longitudinal bars, and plain 6 mm Grade 40 transverse ties. The spacing of the lateral ties will be 100 mm, and the concrete cover of the longitudinal reinforcement on all sides will be kept constant at 20 mm for all specimens.

5. Formwork Setup and Preparation of Specimens

An electric vibrator was used at every level to compact the concrete and remove air bubbles. The concrete had good workability (slump = 200 mm) with a maximum aggregate size of 10 mm. Hence, no honeycombing was observed in the specimens, even for the Geogrids confined concrete columns. After casting, all specimens were covered with wet clothes for 28 days. This process was to maintain the specimens under moist conditions. Specimens were removed from the formwork after 14 days, but remained covered with wet clothes for the next 14 days.

6. Instrumentation and Testing

The specimens were tested in displacement control at a slow rate using 2,000 kN capacity 4-column universal Tinius Olsen testing machine. The displacement level was increased in prescribed increments until specimen failure. The axial strain is measured using six linear variable differential transducers (LVDTs) supplied by Omega Engineering, Stamford, Connecticut. Average axial strains will be measured using four linear variable differential transducers (LVDT) attached to the specimens on either side and positioned over a gage length of 230 mm in the central portion of the specimens. Average axial strains are measured over the full height of the specimens (gage length =

500 mm) using one LVDT attached between the actuator head and the specimen support.

The load is applied in stroke control at an approximate average rate of 1.0 mm/minute. All data including applied load and LVDT readings are monitored using computerized data acquisition system. Schematic of the test setup is shown in Figure **Error! Reference source not found.**.

7. Preliminary tests

Three concrete cylinders with 150 mm in diameter and 300 mm in height were tested for concrete compressive strength on 7 and 28 days. The average compressive strengths on 7 and 28 days were 9 and 11 MPa, respectively.

Tensile properties of the Geogrid were determined by testing several Geogrid strands using the Tenus Olson machine, as shown in Figure **Error! Reference source not found.**. Each end of the Geogrid strand was embedded in steel clamps. The two steel plates were then tightened towards each other in order to fix the Geogrid. The total length of the uniaxial Geogrid strand was 200 mm with a free length of 100 mm. The total length of the biaxial Geogrid strand was 150 mm with a free length of 100 mm. The displacement-controlled test was carried out at a rate of 3 mm/min. The load and deformation data were recorded using an electronic data-logger connected to a computer for every 2 s. The recorded deformation was used to calculate the average tensile strain of the Geogrid. Three coupons were tested for each type of Geogrid. The axial tensile load-axial tensile strain curves of Geogrid have been shown in Figure **Error! Reference source not found.**. For Uniaxial Geogrid, a nonlinear behaviour was observed, while for biaxial Geogrid, a linear elastic behavior was observed. The average ultimate tensile load was approximately 1.43 kN for Uniaxial Geogrid and 1.21 kN for

biaxial Geogrid. The average tensile strength was approximately 233 MPa with an elastic modulus of 81 GPa for biaxial Geogrid, while the average tensile strength was 484 MPa with an elastic modulus of 174 GPa for Uniaxial Geogrid.

A direct tension test is applied to the different types of Geogrids, to get its stress strain curve. This will be used in defining the behavior of the geogrids in the analytical model. View of the direct tension test is shown in Figure **Error! Reference source not found.**. Results of the tests on the uniaxial and biaxial geogrids to be used in the study are shown in Figure **Error! Reference source not found.** and 22.

Figure 19 Direct tension test on (a) Uniaxial Geogrid (b) Biaxial Geogrid

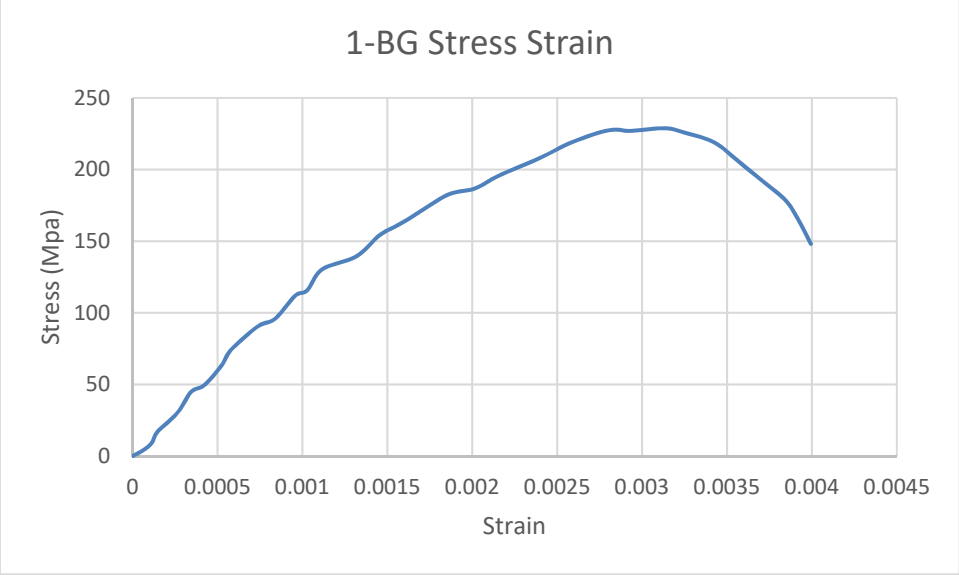

Figure 20 Stress-strain curve of the biaxial Geogrids

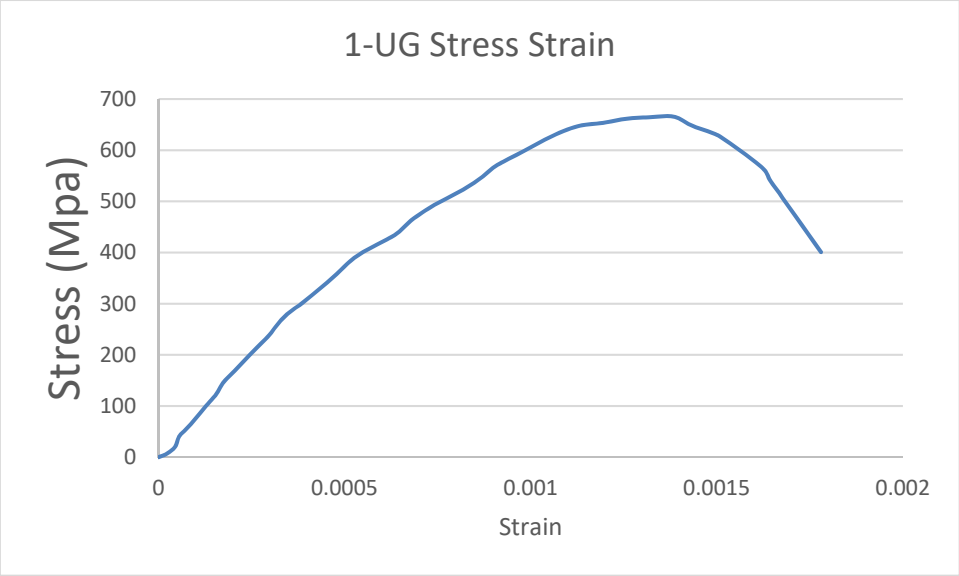

Figure 21 Stress-strain curve of the uniaxial geogrid

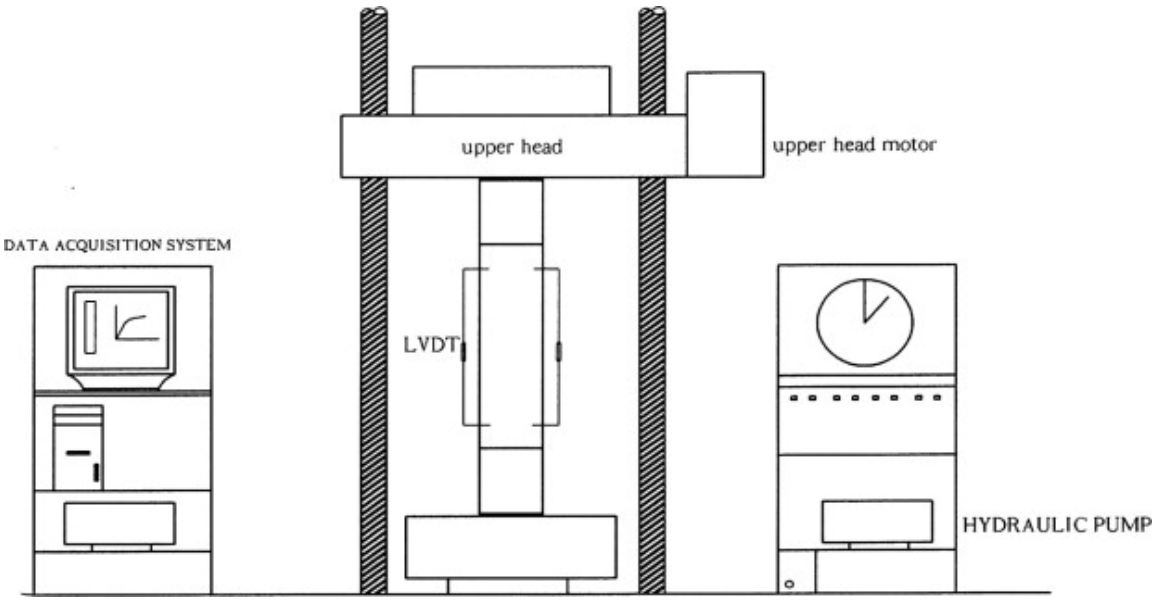

Figure 22 Schematic diagram of the test setup for the tested columns

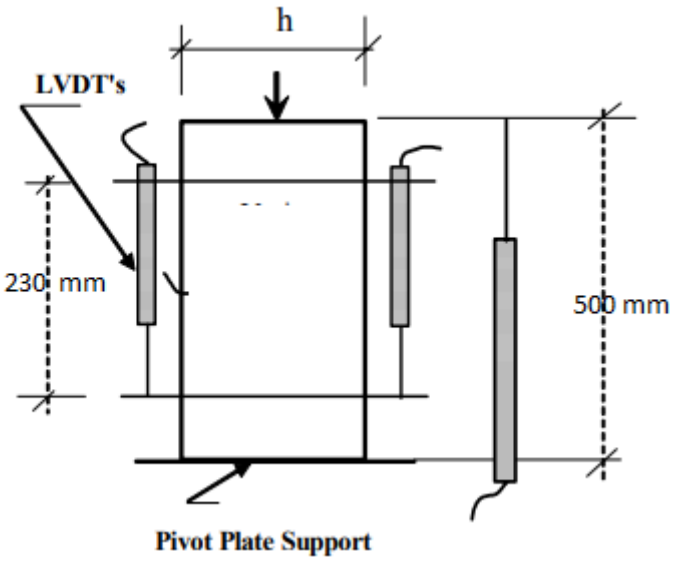

Figure 23 Typical layout of instrumentation

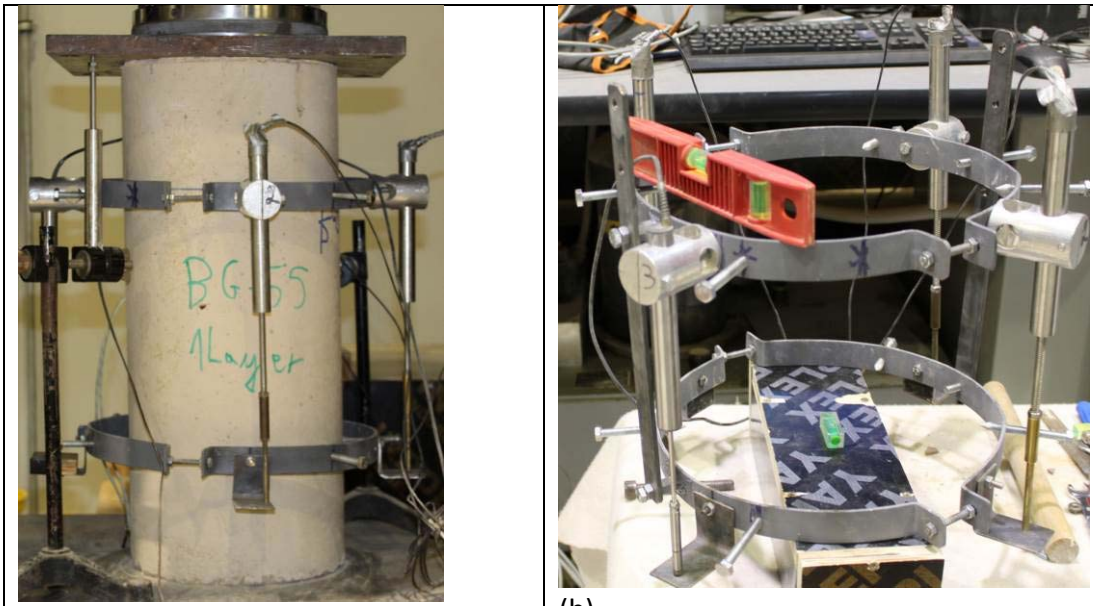

Figure 24 Testing set up

D. EXPERIMENTAL PROGRAM AND TEST VARIABLES

1. Test Variables

Three parameters that may affect the structural behavior of confined columns are evaluated. These parameters are the type of confining material, the column slenderness ratio and the number of confining layers.

a. Confining material

The purpose of this part is to check the efficacy of the use of Geogrid as internal confinement. It is also designated to identify the better Geogrid type as it compares between Biaxial Geogrid confined concrete columns and Uniaxial Geogrid confined concrete columns. In addition, steel stirrups confined concrete columns of different spacing are done to evaluate Geogrid effectiveness as a confining material.

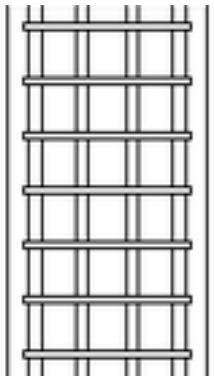

Figure 25 Schematic representation of concrete cylinders with hoop transverse reinforcement

b. Number of Confining Layers

In order to check the effect of the number of confining layers on the confinement effectiveness, the number of confining layers varied one and two layers and all other variables are held constant. An overlap equal to half the perimeter of the cylinder is provided for all the samples.

c. Column Aspect Ratio

The effect of the aspect ratio will be checked by providing different lengths to the specimens while keeping the same diameter. The different aspect ratios checked are: 1.5, 2, 2.5 and 3. The columns are made of plain concrete and are wrapped with one layer of hemp with an overlap equal to half the perimeter of the cylinder in all cases.

2. Preparation of Column Specimens

a. Concrete Mix

Low strength concrete was used throughout the study. Ready-mix concrete was chosen over the conventional mix because of the large amount of concrete needed and since concrete itself is not the main focus of the study. The only requirement is that the concrete have low strength in order to meet with the loading capacity of the machine. All the thirty-six columns were cast vertically from one batch of concrete. The specimens were thoroughly vibrated using a rod vibrator. At the same time, small cylinders (150 mm diameter and 300 mm height) were cast in order to monitor the concrete strength at 7, 28 days and at the time of testing of the columns. After 7 days, all specimens' molds were removed and the cylinders were cured until testing. Figure 26 below show curing process.

Figure 26 Casting of concrete columns

Figure 27 Curing of concrete columns

b. Geogrids Preparation

Figure 28 Testing set up

c. Uniaxial Compression Test Procedure

Four linear variable displacement transducers (LVDTs) were placed on each column. The LVDTs were positioned 90˚ opposite from each other and placed at the middle of each cylinder. Axial compression test was done on all samples using a Tenus Olson machine with a constant displacement rate of 1 mm/min. All the specimen were

axially compressed up to failure and the results were collected using a data logging system.

3. Compression test operation

a. Equipment:

Table (61x41x77)

Wooden plate (52x40x1xm)

Metallic plate (37x30x2cm)

Hexagon Nut

Hexagon Screw

Wooden box (35x11x9cm)

Crescent Wrench (20 cm)
N#13

Voltmeter

exagonal Screwdriver
7 cm)

Level (20x5x1.5cm)

Marker (14 cm)

LVDT Linear Variable Trans
placement Transducer
(L=38 cm, D=30 cm)

Measuring Tape

Dustpan & Brush

Manual Stacker (1.5x1x2.1m)

Computerized Cement Concrete Compressive Strength Testing Machine (1x1x2.8m)

Cart (92x69x30cm)

Wheelbarrow

b. Standard Method:

1. Move the concrete into an accessible position
2. Move the manual stacker next to concrete cylinder
3. Put concrete cylinder on wooden plate on the manual stacker
4. Move the manual stacker next to the compressor
5. Lift the wooden plate (on the manual stacker)
6. Check the voltage inside the concrete using the voltmeter
7. Set up the LVTP
8. Install the LVTP on the concrete cylinder.
9. Put the concrete cylinder on the compressions table
10. Move the manual stacker away
11. Adjust compressor to concrete
12. Input relevant data on the computer connected to compressor
13. Start compression testing

14. Remove LVTP and place on table

15. Move the manual stacker to the compressions table

16. Put the concrete on the manual stacker

17. Move stacker to cart

18. Lower cylinder

19. Put the concrete on the cart

20. Clean the compressions testing station

CHAPTER IV

DISSCUSSION OF TEST RESULTS: BIAXIAL GEOGRIDS CONFINED CONCRETE COLUMNS

A. INTRODUCTION

In this chapter, test results including the stress versus axial and transverse strains for the plain concrete column specimens, the applied load versus axial and transverse strains for the internally reinforced concrete specimens are presented and evaluated. A summary of the axial load capacity and the axial strain for all specimens is provided in **Error! Reference source not found.**. It should be pointed out that in the early stage of loading, the axial strains measured over a length of 230 mm at the center of the specimens were consistently equal to the average axial strains measured over the full height of the specimen (taking into account the negligibly small strain in the approximately 20 mm concrete cover). Moreover, beyond the axial compression stress at which concrete experienced significant compression cracking over localized zones, corresponding to axial strains between 0.002 and 0.003, the strains measured in the middle portion of the specimens, for several specimens, were not sufficiently accurate to warrant their use and therefore it was necessary to switch to the strains measured over the full height.

B. TEST OBSERVATIONS

Test results, including the measured maximum applied load, concrete compressive strength, axial shortening at maximum load, and measured concrete axial strain at maximum load are given in **Error! Reference source not found.**. Comparing the ultimate load of the unconfined specimen to those confined with BG, result indicates that constraining the lateral dilation of concrete by the use of BG develops a tri-axial

stress state within concrete core, and furthermore leads to the enhancement of the axial load-carrying capacity after reaching peak-load.Three types of failure during the testing procedure:

(a) Explosive: the Geogrid sheet was totally fractured.

(b) Non-explosive: the Geogrid sheet was partially fractured.

(c) Crushing of concrete on both ends of the columns.

The axial stress-strain relationships for all tested specimens are compared in Figure **Error! Reference source not found.**. At failures, it was observed that once the concrete cover spall off, BG lost its anchorage provided by the overlap, and the wires ruptured due to the induced high stress concentration developed in the overlap region.

Test results shown in Figure **Error! Reference source not found.** also indicate that the confinement provided by one layer of BG has the same effect on axial load carrying capacity as that of steel stirrups for specimens S-50-20 and S-50-15, of spacing 20 cm and 15 cm, respectively. Furthermore, the results show that two continuous layers of BG are more efficient than the one layer as indicated by the higher load capacity. This behavior might be attributed to the higher anchorage of the BG in the concrete, causing higher stability of the BG.

All BG confined specimens failed in a ductile mode. Initially longitudinal cracks were developed on the outer surface and then expanded to core concrete area accompanied with a series of rupture sound of the BF junctions. Failure occurred after the majority of the concrete cover spall off, as shown in Figure Figure 6 for the typical specimen BG-50-1L.

C. MODE OF FAILURE

Initially, longitudinal cracks were developed on the outer surface of the concrete specimen and then cracks expanded into the core concrete area accompanied with a series of noisy ruptures of the geogrid junctions. Failure occurred after the majority of the concrete cover was spalled off, the geogrid sheet lost anchorage provided by the overlap, and the sheet wires were ruptured due to the induced high stress concentration developed in the overlap region. Figure 29 shows typical failure of specimens confined with one-layer geogrids. Progressive failure was observed for all geogrid confined concrete specimens. Failure occurred when the concrete core expanded outwards significantly, and the rupture of the polymer grid was significant. It should be noted that for all BG confined concrete specimens, the load carrying capacity was fully exhausted at the end of the test (rupture of BG at the junctions), which indicates that the specimens could not carry more axial load with a larger axial deformation. It was also observed that 50-cm concrete specimens confined with one layer of biaxial geogrids had less amount of intact core concrete after failure as compared with concrete specimens confined with two layers of geogrids.

Figure 29 Typical failures: (a) BG-45-1L, (b) BG-50-1L, and (c) BG-60-1L

D. TEST RESULTS AND ANALYSIS

Test results shown in Table 2 include the measured ultimate axial applied load P_{max}, the ratio of the ultimate load of the tested specimen to that of the control specimen (α), axial deformations δ_y and δ_f, ratio (μ) of axial deformations δ_f to δ_y, fracture energy (F), and the ratio of fracture energies of tested specimen to the control unconfined specimen (K). With reference to the schematic load-displacement Figure 30, δ_y is the axial displacement corresponding to the yield load P_y at which the load-displacement curve becomes non-linear and δ_f is the axial displacement that corresponds to one-half of the maximum load reached.

Two indicators were used to measure ductility of the load-displacement history in this research. Ductility is defined as the ability of a structural system or element to undergo inelastic deformation without substantial loss in resistance. The ratio of axial deformations (μ) was assumed as a first measure of ductility of the load-displacement

behavior and is called the displacement ductility index. Fracture energy in this research is defined the area under the load-deformation curve up to δ_f, (refer to Figure 30 Schematic of load-displacement curve to define the parameters used in Table 2). The ratio (K) of fracture energy of the tested specimen to that of the control unconfined specimen was considered as a second measure of ductility of the load-displacement behavior and is called the energy ductility index. It should be noted that replicate specimens gave very comparable results indicating the validity of the test results.

Table 2 Test results

Specimen ID	Ultimate load P_{max} (kN)	Ratio of ultimate loads α**	δ_y*** (mm)	δ_f*** (mm)	Displacement ductility index μ+	Fracture energy F (N-m)	Energy ductility index K++
C*	465.77	1.000	1.073	4.06	3.784	1346.99	1
BG-50-1L*	456.74	0.981	1.139	9.41	8.262	3585.91	2.662
BG-50-2L*	497.69	1.069	0.976	8.16	8.361	3211.52	2.384
BG-40-1L	455.77	0.979	1.316	8.85	6.725	3100.87	2.302
BG-45-1L	452.52	0.972	1.285	11.04	8.591	4167.8	3.094
BG-55-1L	480.74	1.032	1.319	8.88	6.732	3601.33	2.674
BG-60-1L	451.39	0.969	1.319	11.9	9.022	4792.24	3.558
S-50-5	517.16	1.110	0.89	8.44	9.483	3593.97	2.668
S-50-10*	517.04	1.110	0.99	6.79	6.859	2651.95	1.969
S-50-15	493.21	1.059	1.012	5.15	5.089	1899.9	1.410
S-50-20	492.64	1.058	1.001	5.08	5.075	1860.63	1.381

*Two replicates for this specimen were tested to validate the test results

** α is the ratio of the ultimate load of the tested specimen P_{max} to that of the control specimen C

*** δ_y and δ_f are defined in Figure 30

+ μ is the displacement ductility index and is calculated as the ratio of δ_f to δ_y

++ K is the energy ductility index and is calculated as the ratio of the fracture energy of the tested specimen divided by that of the control specimen C; fracture energy is defined in Figure 30

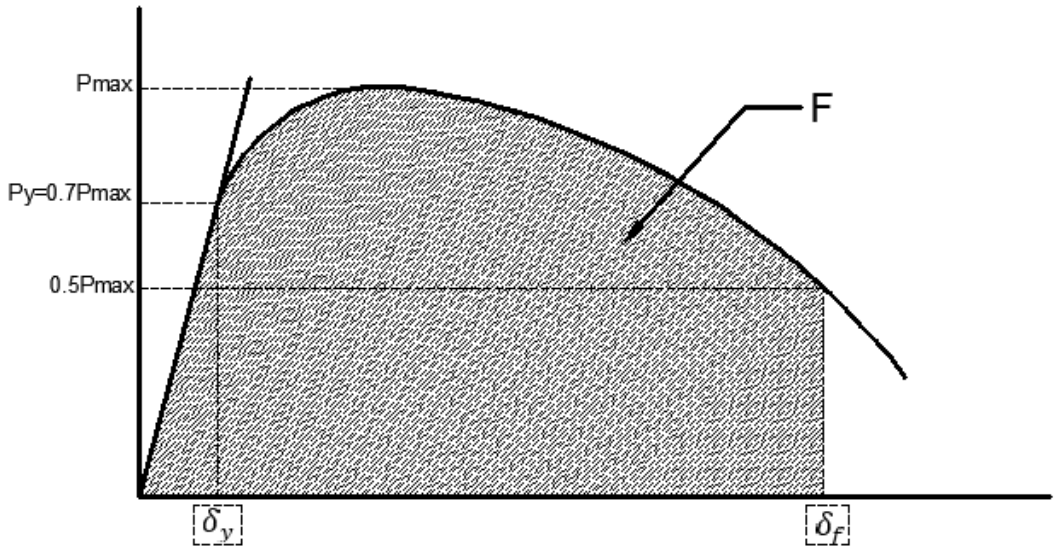

Figure 30 Schematic of load-displacement curve to define the parameters used in Table 2

1. Effect of Number of Geogrid Layers

Figure 31 shows the axial load versus the axial displacement of specimens having constant slenderness ratio and different number of confining geogrid layers: C (unconfined), BG-50-1L and BG-50-2L. The load-displacement behavior starts with a linear portion lasting up to approximately 70% of the ultimate load. Thereafter, the curves enter in a nonlinear stage where large strains begin to be registered for small increments of loads. As compared to the maximum load reached by the control specimen with no confinement, the 1-layer BG specimen dropped by around 2% whereas the 2-layer BG specimen increased by around 7%. The deformation capacity of the two BG confined concrete specimens is much higher than that of unconfined concrete specimen, as reflected by the value of the displacement ductility index μ (refer to Table 2). Another indication of the positive effect of geogrid confinement on energy absorption is the value of the energy ductility index K which is 2.662 for the 1-layer BG

specimen and 2.384 for the 2-layers BG, as compared to the unconfined concrete specimen C.

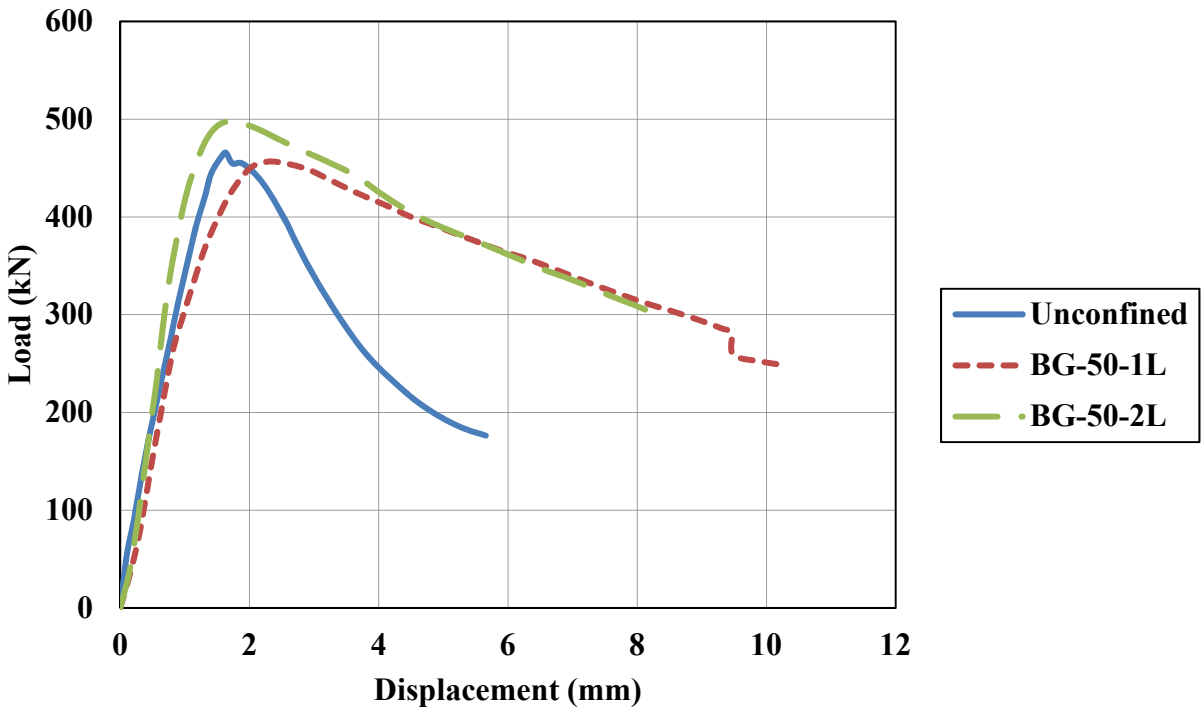

Figure 31 Effect of number of biaxial geogrid layers on load-displacement history

2. *Effect of Slenderness Ratio of the Tested Specimen*

The failure modes of the BG confined specimens with different slenderness ratios are very similar (refer to Figure 32). The specimens failed by the formation of a series of cracks in the cover parallel to the axial direction of loading with a loud bursting noise. The increase in the hoop deformation of the concrete enforces tensile pressure on the BG sheet that leads to the cracking map of the BG at a load very close to failure. Once the ultimate tensile strain of the BG sheet was reached, failure of the concrete specimen occurred in an explosive manner with a sudden release of the stored energy causing small pieces of concrete to be shattered in all directions. After failure, all the loose concrete pieces from the cover were removed and a typical conical concrete

shape appearance was clearly recognized. The delaminated BG sheets were also examined, and it was found that some chunks of concrete were still attached to the column core. This indicates that the bond between concrete and BG sheet is very good.

The axial load-displacement curves of BG confined concrete specimens with different slenderness ratios, presented in Figure 33, indicate no difference in load-displacement behavior. As compared with the unconfined control specimen C, specimens confined with 1-layer BG and different slenderness ratios had ultimate load ratios ranging between 0.969 and 1.032, indicating no significant difference in ultimate load capacity (refer to Table 2 Test results). However, values of the displacement ductility index μ ranged between 6.725 and 9.022 as compared with 3.784 for the unconfined specimen, and values of the energy ductility index K ranged between 2.302 and 3.558 indicating significant increase in energy absorption of BG confined specimens with different slenderness rations relative to the unconfined specimen C.

Figure 32 Failure of specimens with different slenderness ratios

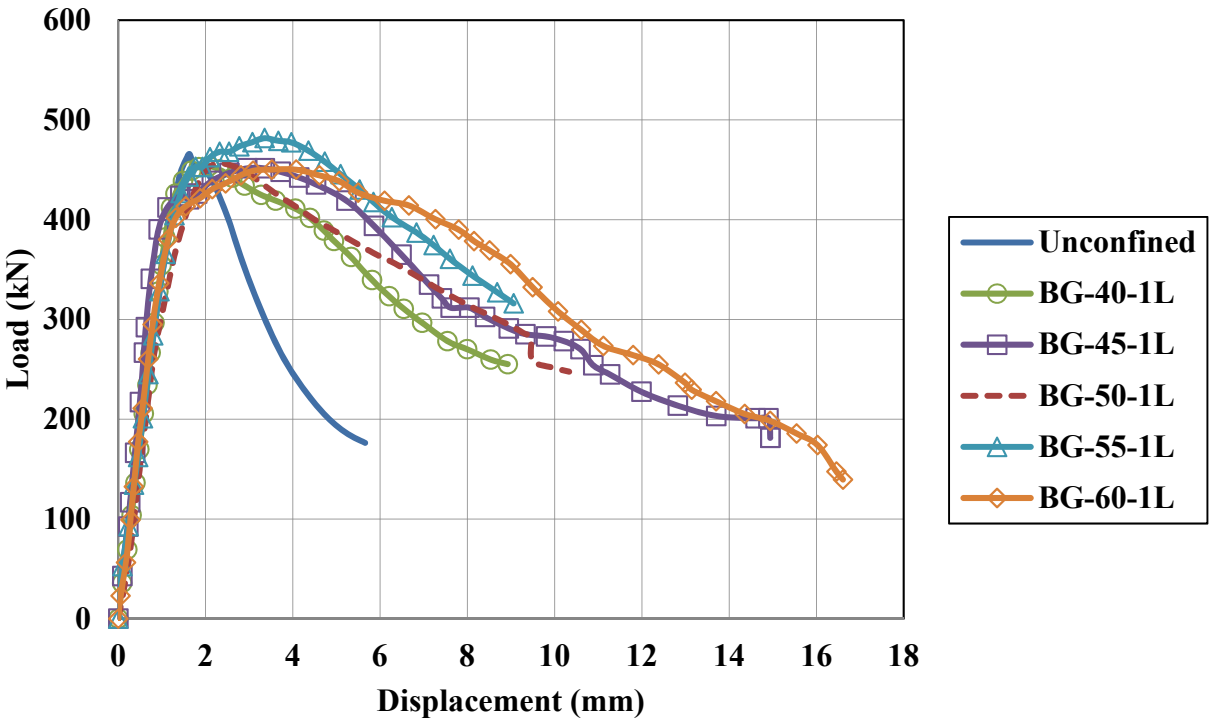

Figure 33 Effect of slenderness ratio on load-displacement history

3. *Effect of the Stirrups Spacing*

Figure 34 shows a plot of the axial compressive load versus the axial displacement of column specimens having constant slenderness ratio but with different stirrups spacing. Specimens S-50-20, S-50-15, S-50-10 and S-50-5 had ties spaced at 200, 150, 100 and 50 mm, respectively. Ultimate loads of the 150 and 200 mm tie spacing specimens improved by around 6% relative to the unconfined specimen, whereas the increase was 11% for the 50 and 100 mm spacing (refer to Table 2 Test results). The positive effect of stirrup confinement is also indicated by the load-displacement history beyond the ultimate load. As compared to the displacement ductility index of the unconfined specimen C (3.784), the values ranged between 5.075 for the 200-mm stirrup spacing to 9.483 for the 50-mm specimen. The energy ductility index ranged from 1.381 to 2.668.

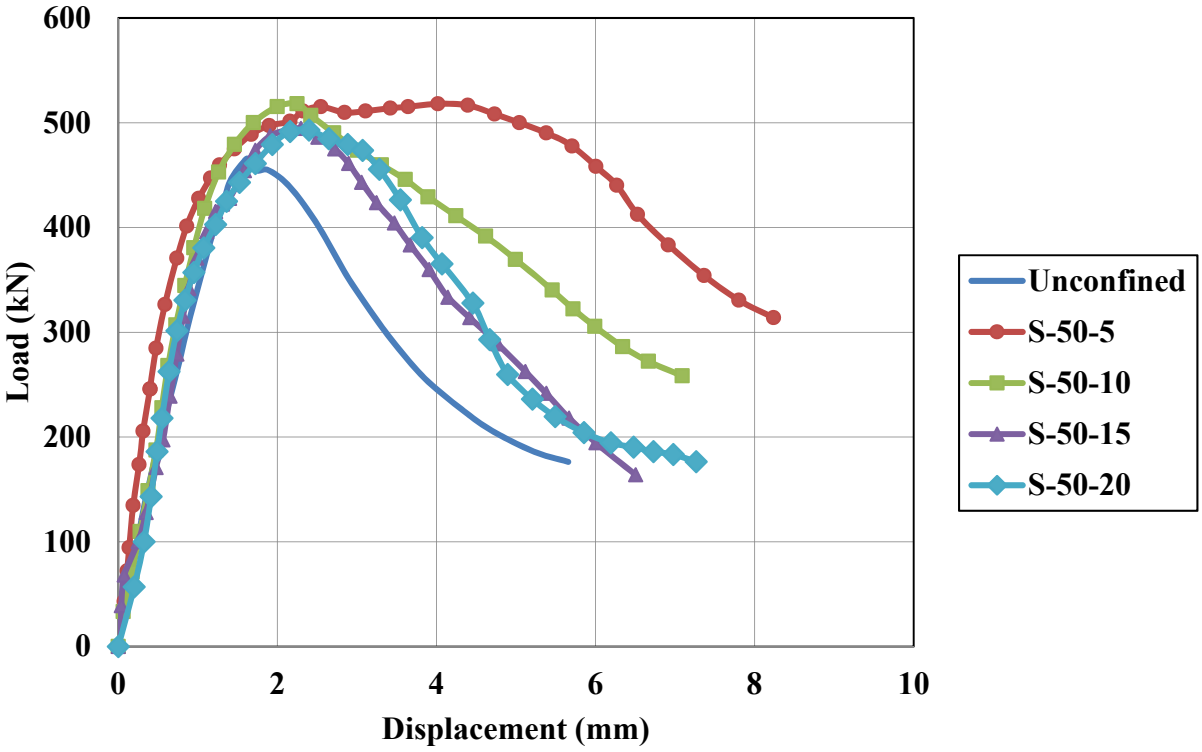

Figure 34 Effect of stirrups spacing on load-displacement history

4. *6.4 Effect of Confinement Type*

In the absence of internal confinement, failure of the concrete specimen was preceded by crushing of the concrete and full buckling of the longitudinal steel bars as shown in Figure 35. The presence of closely spaced stirrups (50 and 100 mm spacing) or biaxial geogrid sheets not only provided confinement of the concrete, but also prevented buckling of the steel bars, leading to better performance.

Referring to the maximum axial load reached, values listed in Table 2 indicate that the 1-layer BG specimens recorded slight decreases (with the exception of BG-60-1L) as compared to the control unconfined specimen. However, the 2-layer specimen recorded a 7% increase which is very similar to the 6% increase of the 150 and 200-mm

stirrup spacing specimens. The 50 and 100-mm stirrup spacing specimens performed best and recorded an 11% increase in the maximum load.

Ductility indexes listed in Table 2 are plotted in Figure 37 and Figure 38. The two plots clearly indicate that geogrid confinement was more effective in improving the ductility of the load-displacement behavior as compared to the 200 or 150-mm stirrups confined specimens. The 100 and 50-mm stirrup spacing specimens had similar performance as the BG specimens. These results prove that although geogrid confinement could decrease slightly the maximum axial load of the column specimen, however the improvement in ductility due to the continuous confinement provided to the column core is significant and is comparable to specimens with very closely spaced stirrups.

Figure 35 Effect of confinement on buckling of longitudinal steel bars (a) P, (b) S-50-15, (c) BG-50-2L

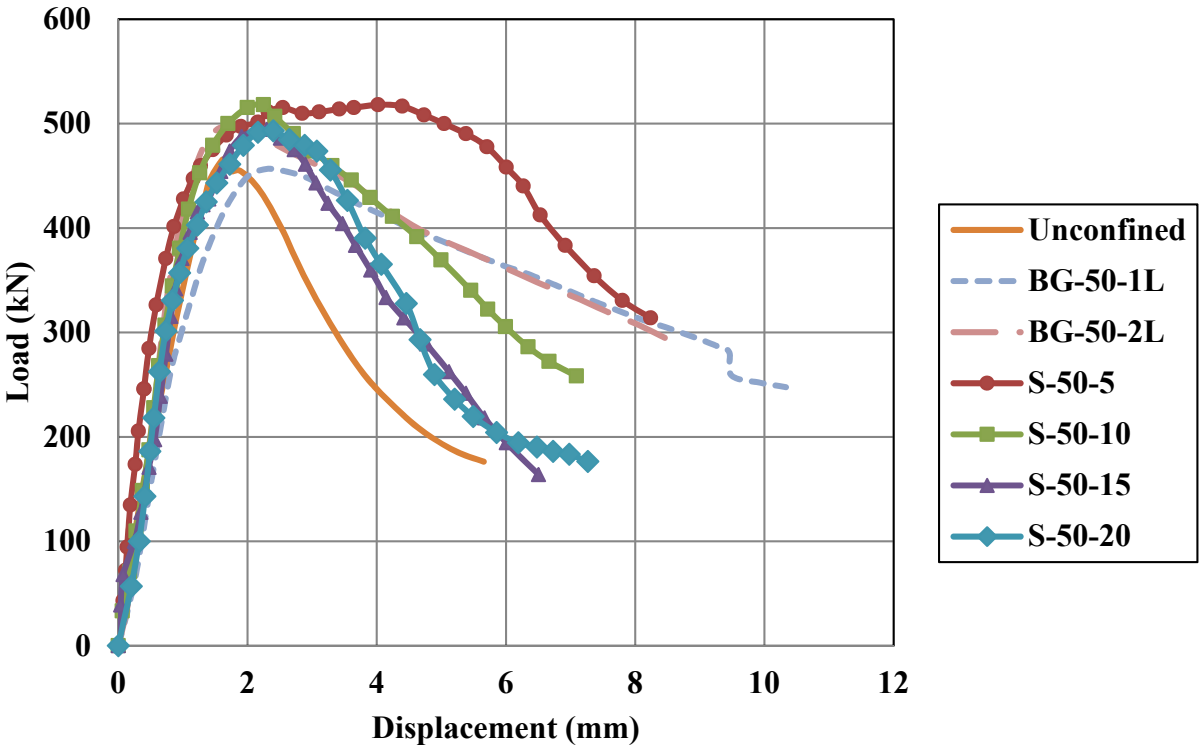

Figure 36 Effect of confinement type on load-displacement history

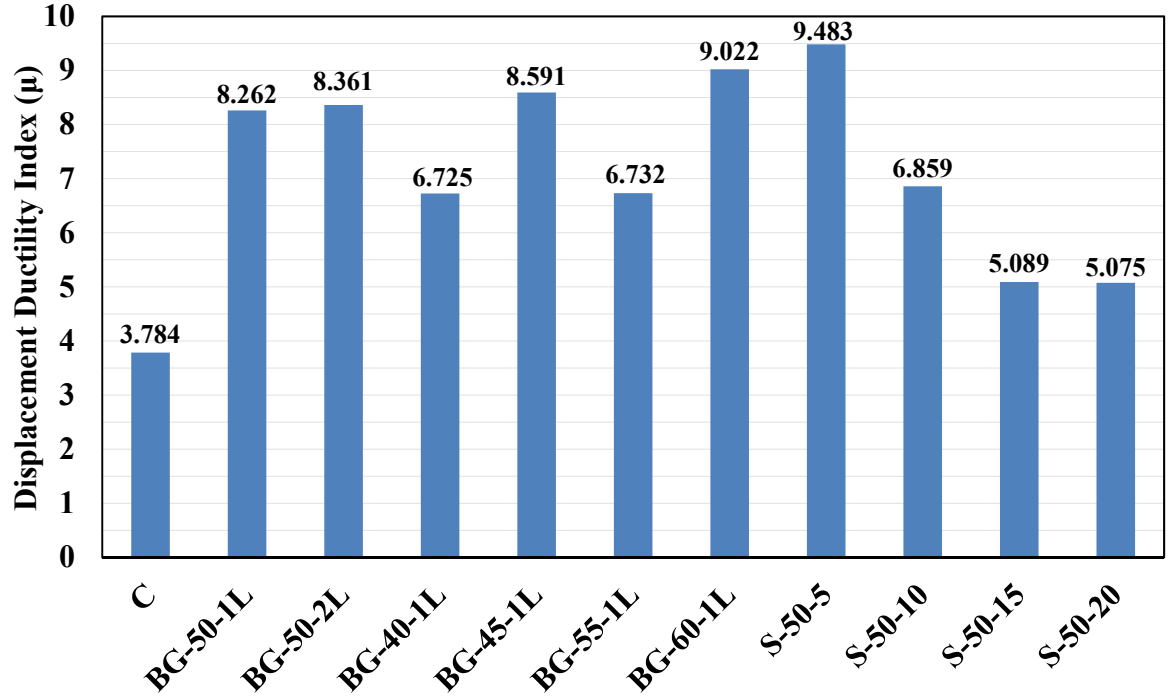

Figure 37 Variation of Displacement Ductility Index (μ) as measured by the ratio of axial displacements δf to δy

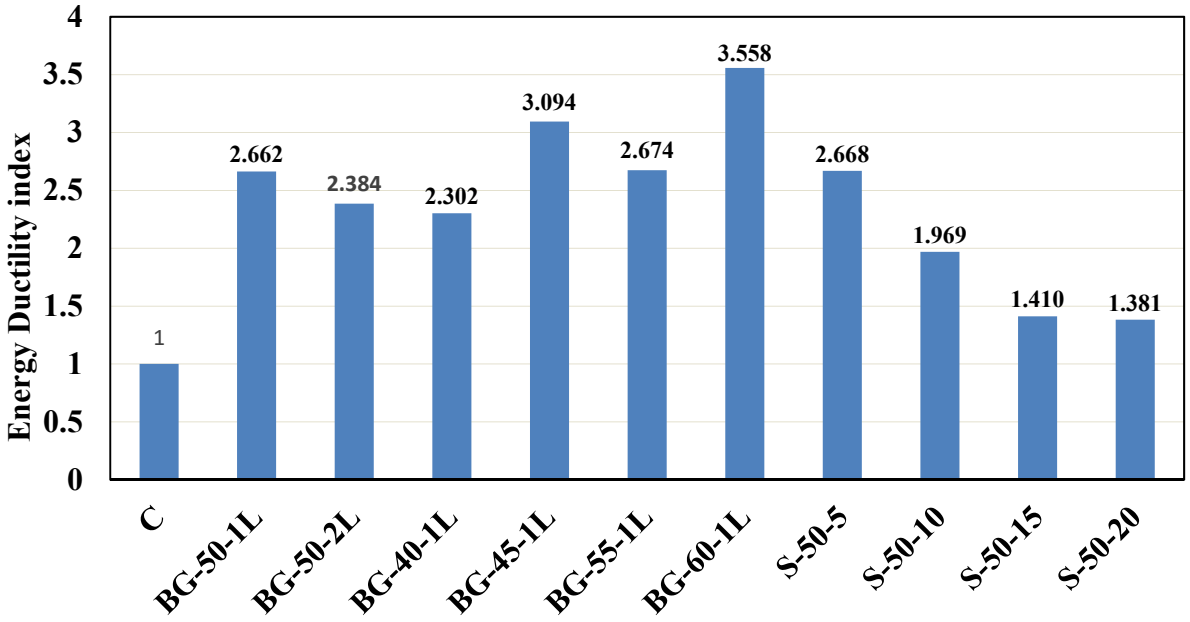

Figure 38 Variation of Energy Ductility Index (K) as measured by the ratio of fracture energies

7. CONFINEMENT MODEL

Very limited research investigates the development of stress–strain models to predict the axial compressive behavior of Geo-polymer sheets confined concrete. The present study approaches all geogrid reinforced concrete columns that are being designed in highly corrosive environment. Biaxial geogrid (BG) is one of the materials being evaluated as potential reinforcement. Most models for concrete confined with BG reinforcement are based on the fact that a single layer of Geogrids will provide adequate reinforcement to sufficiently confine the concrete. These models were developed to study the behavior of different materials to confine concrete. These are based on a constant thickness of the confining material that fully covers the external surface of the concrete. The cross-rib of the BG only cover part of the area. One approach using these

models is to determine an equivalent full coverage thickness for the rib. The equivalent rib thickness (t_{eq}) was calculated based on the following expression:

$$t_{eq} = \frac{n_l.n_r.b_r.t_r}{h} \quad (1)$$

Where: n_l the number of BG layers,n_r is the number of ribs, b_r is the width of the rib, t_r is the thickness of the rib and h is the height of the specimen. For columns or other concrete elements that have large axial lengths, Equation 1 can be simplified as follows:

$$t_{eq} = \frac{n_l.b_r.t_r}{s_r} \quad (2)$$

Where: s_r is the BG ribs spacing. To determine the confinement strength (f_u), the equilibrium condition requires the force from the confining strength be equal to the force in the BG core. The force from confinement is equal to the confining strength times the diameter of the enclosed concrete and the force in the encasement is equal to the strength of the encasement times twice the thickness of the BG encasement. By rearranging the equations, the confinement strength (f_u) was found:

$$f_u = \frac{2.t_{eq}}{d_g} . f_{ru} \quad (3)$$

Where f_u is the confinement strength, d_g is the diameter of the BG sheet and f_{ru} is the ultimate strength of the BG rib. Assuming that the confined concrete is in a

triaxial stress state, the increase in strength provided by the confinement is reflected in the maximum stress (f''_{cc}) for a cylindrical specimen, which is defined by Mander et al. [14] as:

$$f''_{cc} = f'_c + k_1 . f_u \quad (4)$$

Where: k_1 is the confinement effectiveness coefficient. The confinement effectiveness coefficient for concrete confined by steel is usually taken between 2.8 and 4.1. Campione and Miraglia [15] found that the above values overestimate the confinement effectiveness coefficient for concrete wrapped with FRP and some other confining material. For the purpose of this study the confinement effectiveness coefficient was taken as 2. The axial strain of confined concrete at the peak stress (ε_{co}) was determined in a similar manner as unconfined concrete using the following expression of Wight and MacGregor [16]:

$$\varepsilon_{co} = 1.8 \cdot \frac{f''_{cc}}{E_c} \quad (5)$$

Equations (4) and (5) were combined with the modified Hognestad stress-strain equation [17] as follows:

$$f_c = f''_{cc} \cdot \left[\frac{2 \cdot \varepsilon_c}{\varepsilon_{co}} - \left(\frac{\varepsilon_c}{\varepsilon_{co}}\right)^2\right] \quad (6)$$

$$f_c = f''_{cc} \cdot [1 - D_c \cdot (\varepsilon_c - \varepsilon_{co})] \quad (7)$$

Where ε_c is the concrete strain, ε_{co} is the strain at peak stress of unconfined concrete and ε_{cu} is the ultimate strain. These equations are plotted in Figure 15. The modified Hognestad equations model the ascending branch (AB) with a parabolic relationship and the descending branch BC with a linearly descending curve. The equation for region BC is based on the deterioration constant (D_c) that controls the slope of the line.

$$f_c = f''_{cc} \cdot \left[\left[\frac{2 \cdot \varepsilon_c}{\varepsilon_{co}} - \left(\frac{\varepsilon_c}{\varepsilon_{co}}\right)^2\right] \cdot H(\varepsilon_{co}) + [1 - D_c \cdot (\varepsilon_c - \varepsilon_{co})] \cdot H(\varepsilon_{co} - \varepsilon_c)\right] \quad (8)$$

The material properties of the BG ribs were used to construct the stress-strain curve of the BG confined concrete. The average strength of the control cylinders tested in displacement control mode was taken as the strength of unconfined concrete (f'_c). An average BG sheets diameter of 200 mm was used. The ultimate concrete strain ε_{cu} was assumed to be 15000 micro strains. The average stress-strain curve for the BG confined concrete was constructed using data from all tested columns. The deterioration constant was taken equal to 50 to match post peak experimental data. All three curves are depicted in Figure 40 and Figure 41. The modified Hognestad matches well with the experimental curve.

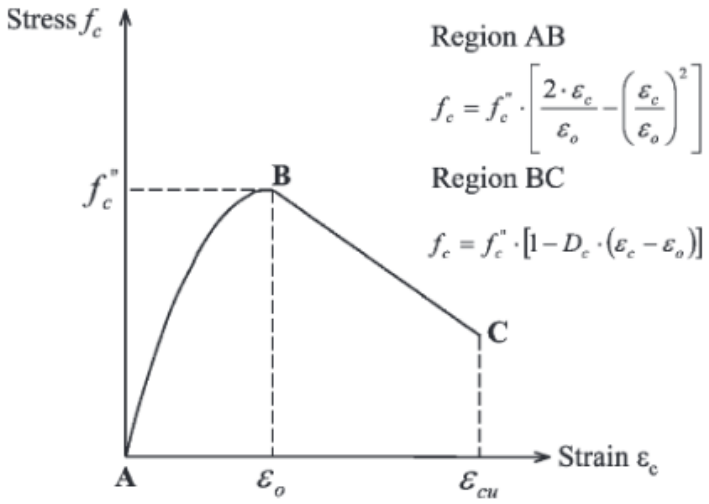

Figure 39 Modified Hognestad Stress Strain-Curve; Park and Pauly

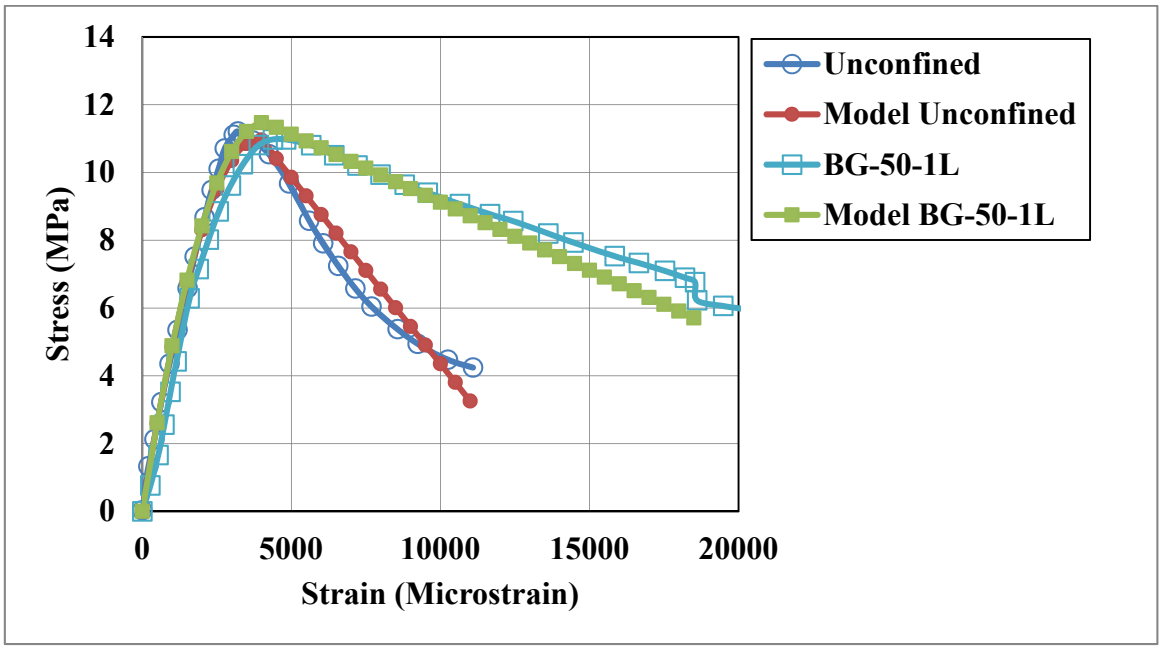

Figure 40 Experimental and Modified Hognestad Model stress-strain curves of unconfined and 1-layer BG confined specimens

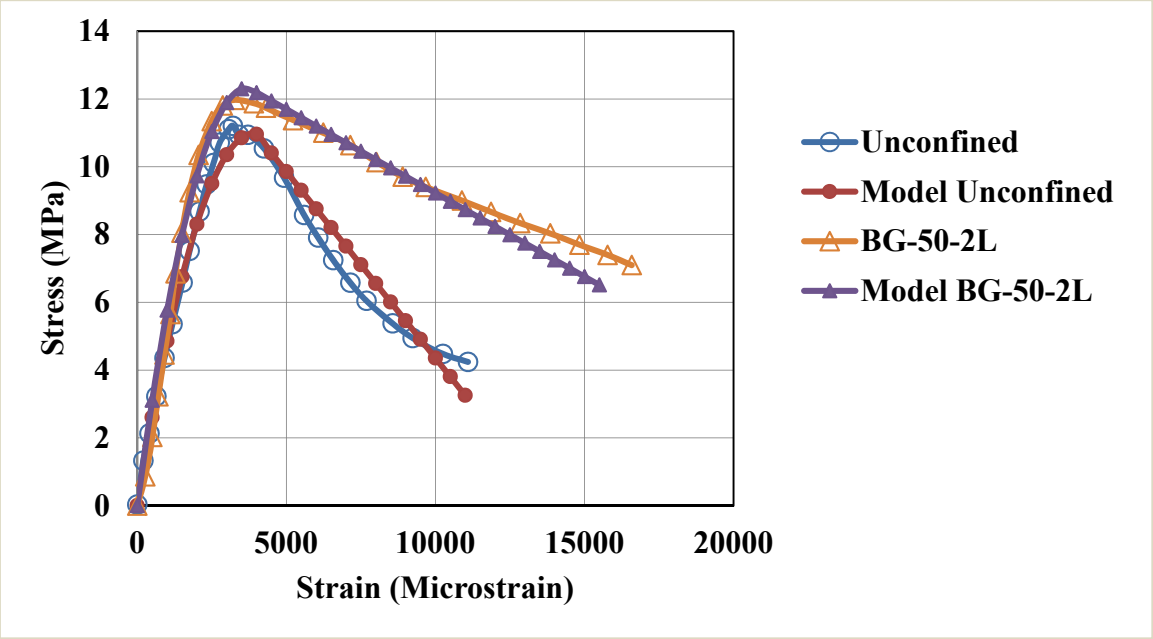

Figure 41Experimental and Modified Hognestad Model stress-strain curves of unconfined and 2-layer BG confined specimens

CHAPTER V

DISSCUSSION OF TEST RESULTS: UNIAXIAL GEOGRIDS CONFINED CONCRETE COLUMNS

A. EXPERIMENTAL RESULTS AND DISCUSSION

1. Test observations

Test results, including the measured maximum applied load, concrete compressive strength, axial shortening at maximum load, and measured concrete axial strain at maximum load are given in **Error! Reference source not found.**. Comparing the ultimate load of the unconfined specimen to those confined with UG, result indicates that constraining the lateral dilation of concrete by the use of UG develops a tri-axial stress state within concrete core, and furthermore leads to the enhancement of the axial load-carrying capacity. Three types of failure during the testing procedure:

a. Explosive: the Geogrid sheet was totally fractured.
b. Non-explosive: the Geogrid sheet was partially fractured.
c. Crushing of concrete on both ends of the columns.

The axial stress-strain relationships for all tested specimens are compared in Figure 8. At failures, it was observed that once the concrete cover spall off, UG lost its anchorage provided by the overlap, and the wires ruptured due to the induced high stress concentration developed in the overlap region.

Test results shown in Figure 9 also indicate that the confinement provided by one layer of UG has the same effect on axial load carrying capacity as that of steel stirrups for specimens S-50-10, of spacing 10 cm. Furthermore, the results show that two continuous layers of UG are more efficient than the one layer as indicated by the

higher load capacity. This behavior might be attributed to the higher anchorage of the UG in the concrete, causing higher stability of the UG.

All UG confined specimens failed in a ductile mode. Initially longitudinal cracks were developed on the outer surface and then expanded to core concrete area accompanied with a series of rupture sound of the UF junctions. Failure occurred after the majority of the concrete cover spall off, as shown in Figure 6 for the typical specimen UG-50-1L.

2. Failure mode

The failure mode of the concrete cylinders, with various confinement materials, is presented in Figure 42. The unconfined concrete cylinder experienced gradual vertical cracking before failure, breaking into individual fragments at the end of the loading. This brittle failure was indicative of the lower ductility of unconfined concrete cylinder. S-50-10 and S-50-5 cylinders failed due to sudden crushing of concrete core in the form of a single vertical crack. In the case of UG confined concrete, the presence of UG sheets led to gradual rupture of the UG sheets which maintained the integrity of the concrete core.

The spalling of concrete cover for Geogrids confined concrete specimens was first observed during the test, which resulted in a higher axial peak load than that of plain concrete specimens. As the concrete cover thickness (20 mm) was higher than the maximum aggregate size (9.8 mm) of the concrete, the integrity of the concrete cover was satisfactory, which caused the spalling of concrete cover at the peak loading stage. Figure 9 shows the representative failure modes of Geogrid confined concrete specimens after tests. Progressive failure was observed for all Geogrid confined concrete specimens. As can be seen from Figure 42, the concrete core expanded

outwards significantly. Not all Geogrids was fractured for uniaxial Geogrid confined concrete specimens. While for biaxial Geogrid confined concrete specimens, the rupture of UG was significant, resulting in the failure of the specimens. In addition, for concrete specimens confined with one layer of Geogrid, less amount of concrete core remained intact after failure. For concrete specimens confined with two layers of Geogrid, larger amount of concrete remained undamaged within the concrete core after failure.

Figure 42 Typical failures: Crushing of concrete (a) UG-50-2L (b) UG-45-1L, Rupture of UG (c) UG-50-1L

B. TEST RESULTS AND ANALYSIS

Test results shown in Table 3 include the measured ultimate axial applied load P_{max}, the ratio of the ultimate load of the tested specimen to that of the control specimen (α), axial deformations δ_y and δ_f, ratio (μ) of axial deformations δ_f to δ_y, fracture energy (F), and the ratio of fracture energies of tested specimen to the control unconfined specimen (K). With reference to the schematic load-displacement Figure 43, δ_y is the axial displacement corresponding to the yield load P_y at which the load-displacement

curve becomes non-linear and δ_f is the axial displacement that corresponds to one-half of the maximum load reached.

Two indicators were used to measure ductility of the load-displacement history in this research. Ductility is defined as the ability of a structural system or element to undergo inelastic deformation without substantial loss in resistance. The ratio of axial deformations (μ) was assumed as a first measure of ductility of the load-displacement behavior and is called the displacement ductility index. Fracture energy in this research is defined the area under the load-deformation curve up to δ_f, (refer to Figure 30 Schematic of load-displacement curve to define the parameters used in Table 2). The ratio (K) of fracture energy of the tested specimen to that of the control unconfined specimen was considered as a second measure of ductility of the load-displacement behavior and is called the energy ductility index. It should be noted that replicate specimens gave very comparable results indicating the validity of the test results.

Table 3 Test results

Specimen ID	Ultimate load P_{max} (kN)	Ratio of ultimate loads α**	δ_y*** (mm)	δ_f*** (mm)	Displacement ductility index μ+	Fracture energy F (N-m)	Energy ductility index K++
C	465.22	1.000	1.073	4.06	3.784	1346.99	1.000
UG-50-1L	489.98	1.053	1.200	6.7	5.583	3887.61	2.886
UG-50-2L	527.98	1.135	1.470	12.28	8.354	6490.79	4.819
UG-40-1L	495.83	1.066	1.200	11.8	9.833	4415.66	3.278
UG-45-1L	527.61	1.134	1.506	15.9	10.558	6051.99	4.493
UG-55-1L	529.72	1.139	1.240	13.4	10.806	7193	5.340
S-50-5	517.16	1.112	0.890	8.44	9.483	3593.97	2.668
S-50-10*	517.04	1.111	0.990	6.79	6.859	2651.95	1.969
S-50-15	493.21	1.060	1.012	5.15	5.089	1899.9	1.410
S-50-20	492.64	1.059	1.001	5.08	5.075	1860.63	1.381

*Two replicates for this specimen were tested to validate the test results

∗∗ α is the ratio of the ultimate load of the tested specimen P_{max} to that of the control specimen C

∗∗∗ δ_y and δ_f are defined in Figure 43

+ μ is the displacement ductility index and is calculated as the ratio of δ_f to δ_y

++ K is the energy ductility index and is calculated as the ratio of the fracture energy of the tested specimen divided by that of the control specimen C; fracture energy is defined in Figure 43

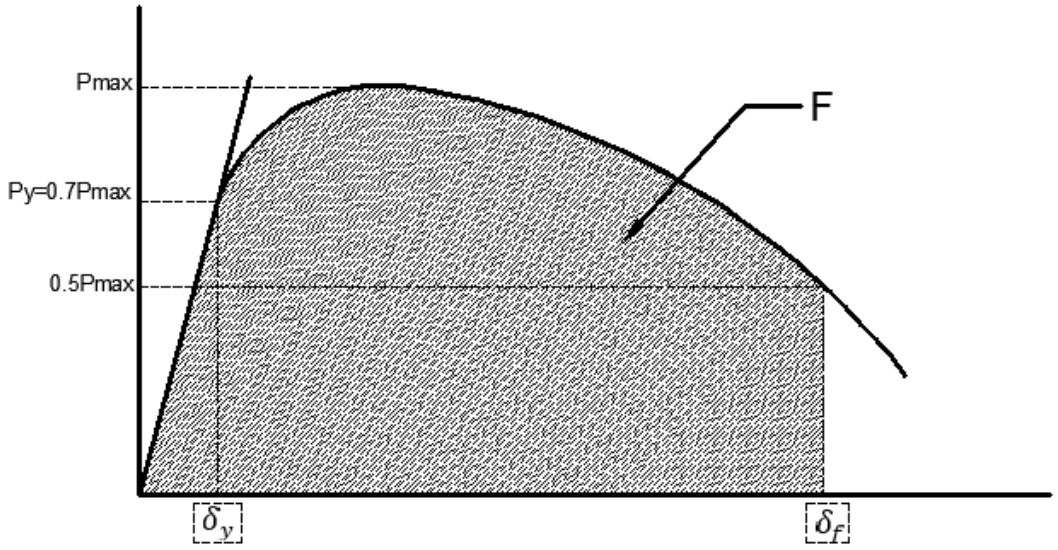

Figure 43 Schematic of load-displacement curve to define the parameters used in Table 3

1. Effect of Number of Geogrid Layers

Figure 44 shows the axial load versus the axial displacement of specimens having constant slenderness ratio and different number of confining geogrid layers: C (unconfined), UG-50-1L and UG-50-2L. The load-displacement behavior starts with a linear portion lasting up to approximately 80% of the ultimate load. Thereafter, the curves enter in a nonlinear stage where large strains begin to be registered for small increments of loads. As compared to the maximum load reached by the control

specimen with no confinement, the 1-layer UG specimen increased by around 5% whereas the 2-layer UG specimen increased by around 11%. The deformation capacity of the two UG confined concrete specimens is much higher than that of unconfined concrete specimen, as reflected by the value of the displacement ductility index μ (refer to Table 2). Another indication of the positive effect of geogrid confinement on energy absorption is the value of the energy ductility index K which is 2.886 for the 1-layer UG specimen and 5.34 for the 2-layers UG, as compared to the unconfined concrete specimen C.

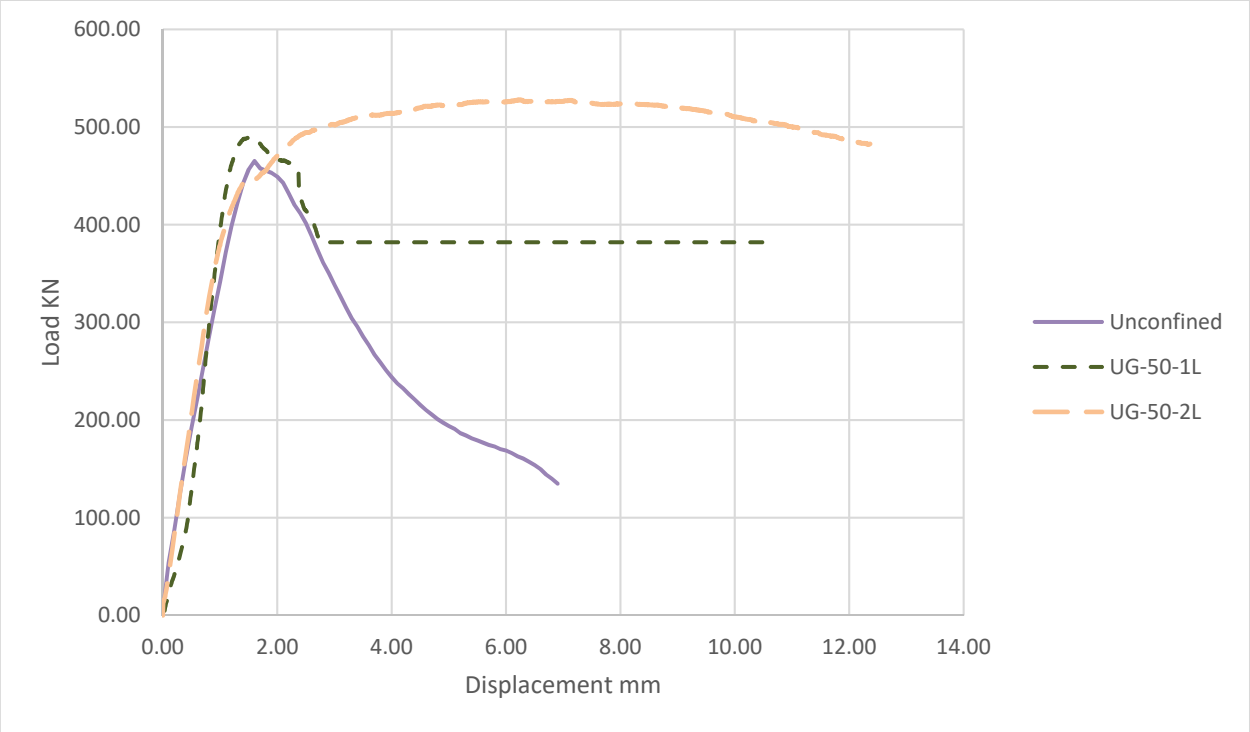

Figure 44 Effect of number of Uniaxial geogrid layers on load-displacement history

2. *Effect of Slenderness Ratio of the Tested Specimen*

The failure modes of the UG confined specimens with different slenderness ratios are very similar (refer to Figure 32). The specimens failed by the formation of a series of cracks in the cover parallel to the axial direction of loading with a loud

bursting noise. The increase in the hoop deformation of the concrete enforces tensile pressure on the UG sheet that leads to the cracking map of the UG at a load very close to failure. Once the ultimate tensile strain of the UG sheet was reached, failure of the concrete specimen occurred in an explosive manner with a sudden release of the stored energy causing small pieces of concrete to be shattered in all directions. After failure, all the loose concrete pieces from the cover were removed and a typical conical concrete shape appearance was clearly recognized. The delaminated UG sheets were also examined, and it was found that some chunks of concrete were still attached to the column core. This indicates that the bond between concrete and UG sheet is very good.

The axial load-displacement curves of UG confined concrete specimens with different slenderness ratios, presented in Figure 33, indicate no significant differences in load-displacement behavior. As compared with the unconfined control specimen C, specimens confined with 1-layer UG and different slenderness ratios had ultimate load ratios ranging between 1.20 and 1.506, indicating increasing in ultimate load capacity (refer to Table 2 Test results). However, values of the displacement ductility index μ ranged between 5.583 and 10.806 as compared with 3.784 for the unconfined specimen, and values of the energy ductility index K ranged between 2.886 and 5.34 indicating significant increase in energy absorption of UG confined specimens with different slenderness rations relative to the unconfined specimen C.

Figure 45 Failure of specimens with different slenderness ratios

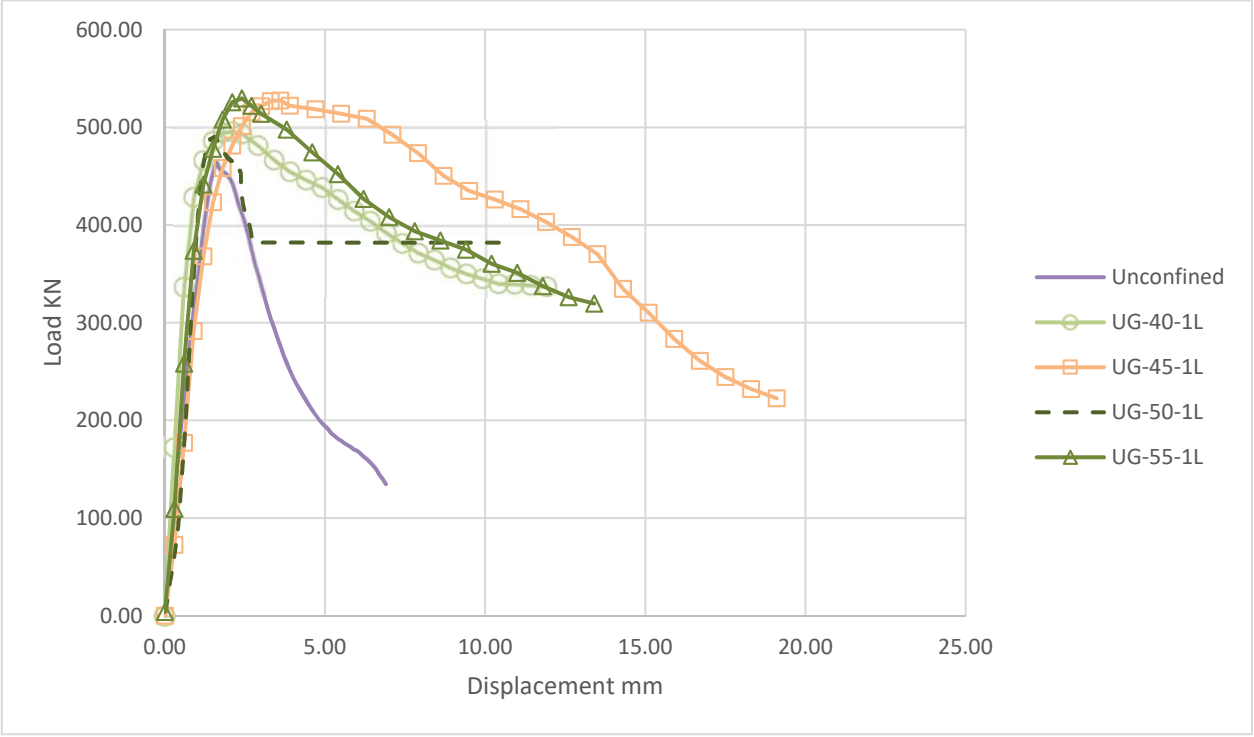

Figure 46 Effect of slenderness ratio on load-displacement history

3. *Effect of the Stirrups Spacing*

Figure 34 shows a plot of the axial compressive load versus the axial displacement of column specimens having constant slenderness ratio but with different stirrups spacing. Specimens S-50-20, S-50-15, S-50-10 and S-50-5 had ties spaced at200, 150, 100 and 50 mm, respectively. Ultimate loads of the 150 and 200 mm tie spacing specimens improved by around 6% relative to the unconfined specimen, whereas the increase was 11% for the 50 and 100 mm spacing (refer to Table 2 Test results). The positive effect of stirrup confinement is also indicated by the load-displacement history beyond the ultimate load. As compared to the displacement ductility index of the unconfined specimen C (3.784), the values ranged between 5.075 for the 200-mm stirrup spacing to 9.483 for the 50-mm specimen. The energy ductility index ranged from 1.381 to 2.668.

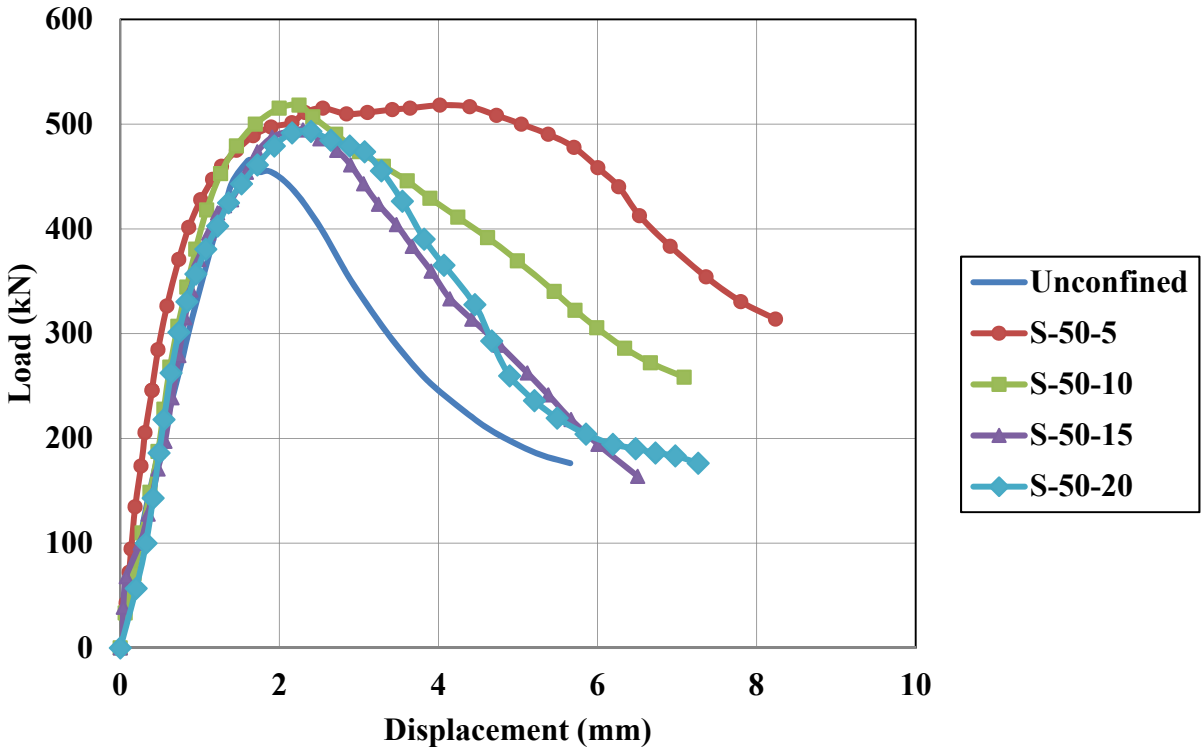

Figure 47 Effect of stirrups spacing on load-displacement history

4. ***Effect of Confinement Type***

In the absence of internal confinement, failure of the concrete specimen was preceded by crushing of the concrete and full buckling of the longitudinal steel bars as shown in Figure 48. The presence of closely spaced stirrups (50 and 100 mm spacing) or biaxial geogrid sheets not only provided confinement of the concrete, but also prevented buckling of the steel bars, leading to better performance.

Referring to the maximum axial load reached, values listed in Table 3 indicate that the 1-layer UG specimens recorded slight increases as compared to the control unconfined specimen. However, the 2-layer specimen recorded a 13% increase which is very similar to the 11% increase of the 50 mm stirrup spacing specimens.

Ductility indexes listed in Table 3 are plotted in Figure 37 and Figure 38. The two plots clearly indicate that geogrid confinement was more effective in improving the ductility of the load-displacement behavior as compared to the 200 or 150-mm stirrups confined specimens. The 100 and 50-mm stirrup spacing specimens had similar performance as the UG specimens. These results indicate the improvement in ductility due to the continuous confinement provided to the column core is significant and is comparable to specimens with very closely spaced stirrups.

(a) (b) (c)

Figure 48 Effect of confinement on buckling of longitudinal steel bars: (a) P(1) (b) S15(2) (c) UG-50-2L(2)

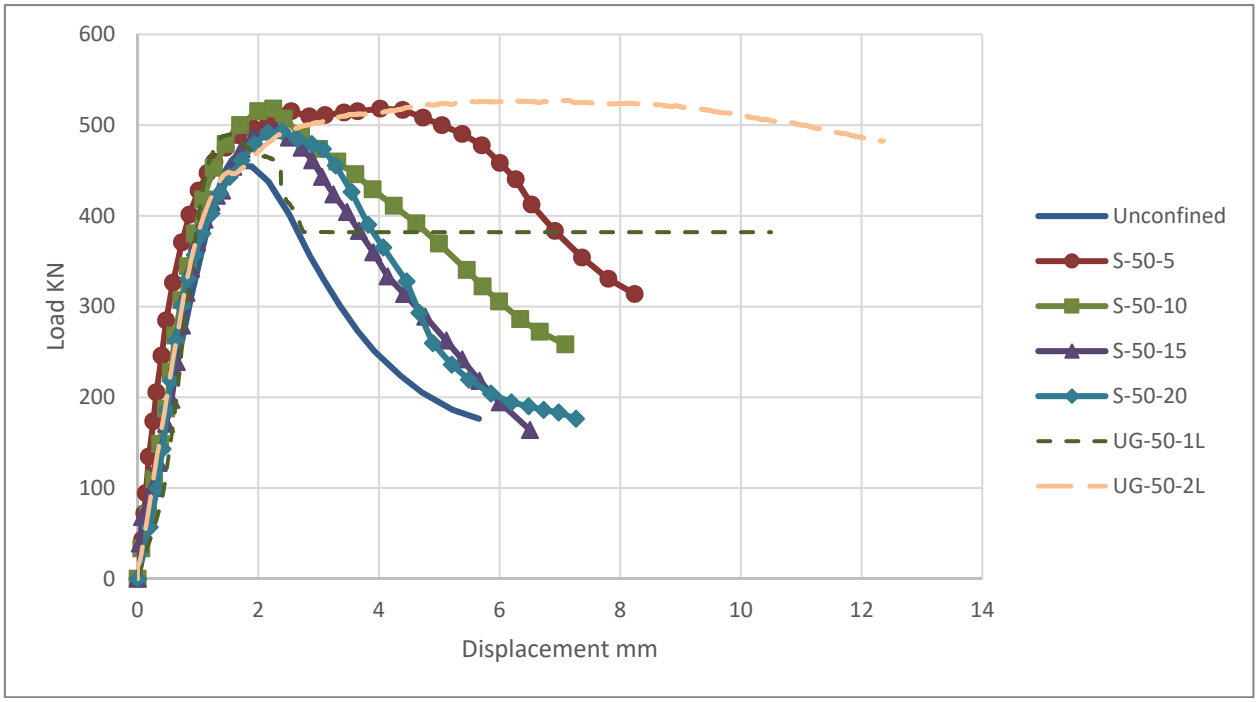

Figure 49 Effect of confinement type on load-displacement history

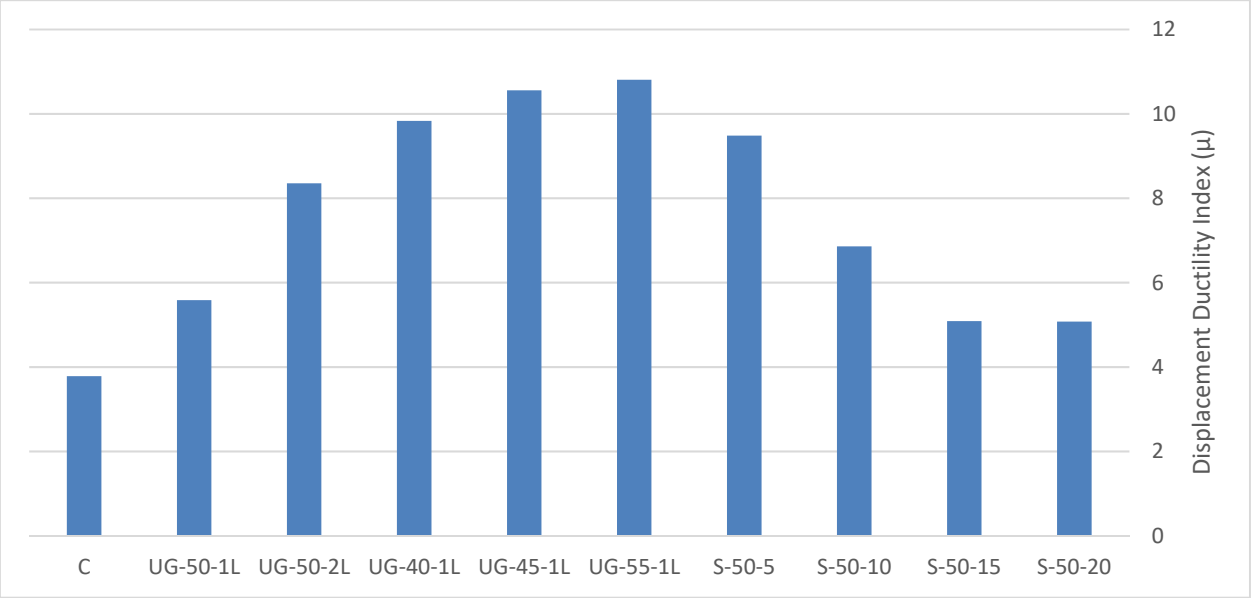

Figure 50 Variation of Displacement Ductility Index (μ) as measured by the ratio of axial displacements δf to δy

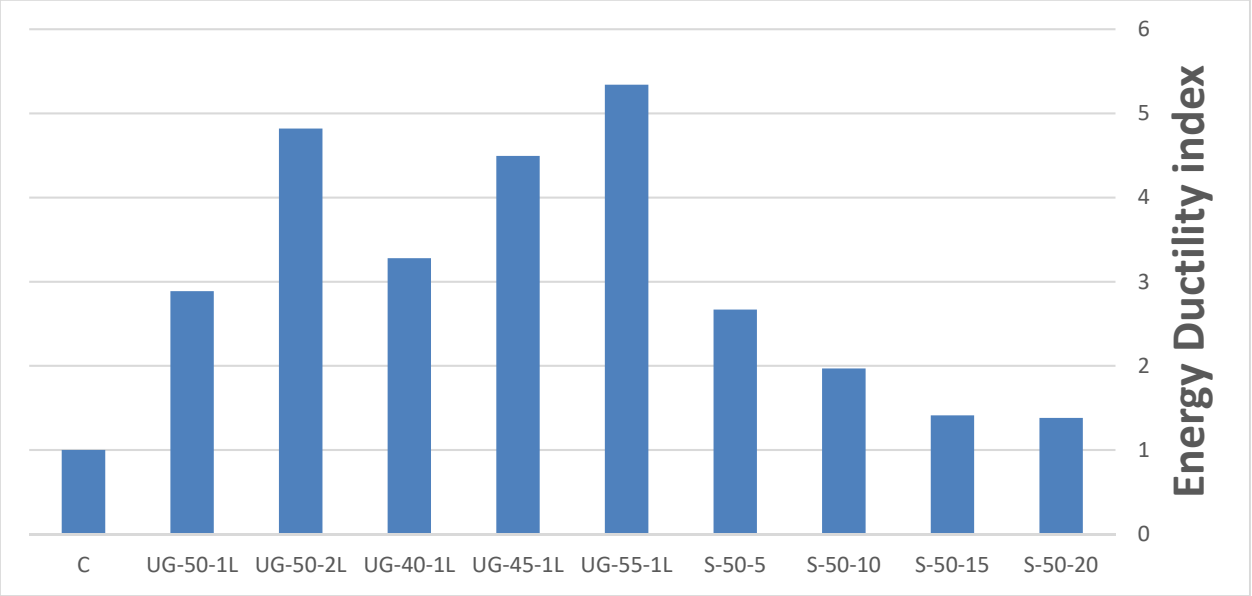

Figure 51 Variation of Energy Ductility Index (K) as measured by the ratio of fracture energies

7. CONFINEMENT MODEL

When the UG is used as confinement reinforcement it is expected that the confining pressure and confinement effectiveness would be less than that of a fully jacketed system.

Several existing models were investigated to model the behavior of different material used to confine concrete. All of the existing models examined are based on a constant thickness of the confining material that fully covers the external surface of the concrete. The cross-rib of the UG only cover part of the area. One approach when using the existing models is to determine an equivalent full coverage thickness for the rib. The equivalent rib thickness (t_{eq}) was calculated based on the following expression:

$$t_{eq} = \frac{n_l.n_r.b_r.t_r}{h} \quad (1)$$

Where: n_l the number of UG layers, n_r is the number of ribs, b_r is the width of the rib, t_r is the thickness of the rib and h is the height of the cylinder. For columns or other concrete elements that have large axial lengths Equation 1 can be simplified as follows:

$$t_{eq} = \frac{n_l.b_r.t_r}{s_r} \quad (2)$$

Where: s_r is the UG ribs spacing.

The secant modulus of elasticity of concrete (Ec) was calculated based on existing empirical expressions (Nawy 2003):

$$Ec = 4730\sqrt{f'c} \quad (3)$$

Where: $f'c$ is the minimum specified compressive strength of concrete, in N/mm^2, at 28 days.

To determine the confinement strength (f_u) simple mechanics were used. The equilibrium condition requires the force from the confining strength be equal to the

force in the UG core. The force from confinement is equal to the confining strength times the diameter of the enclosed concrete and the force in the encasement is equal to the strength of the encasement times twice the thickness of the UG encasement. By rearranging the equation the confinement strength (f_u) was found:

$$f_u = \frac{2.t_{eq}}{d_g}.f_{ru} \quad (4)$$

Where f_u is the confinement strength, d_g is the diameter of the UG sheet and f_{ru} is the ultimate strength of the UG rib.

Assuming that the confined concrete is in a triaxial stress state, the increase in strength provided by the confinement is reflected in the maximum stress (f''_{cc}) for a cylindrical specimen, which is defined as (Mander ET al.1988):

$$f''_{cc} = f'_c + k_1.f_u \quad (5)$$

Where: k_1 is the confinement effectiveness coefficient. The confinement effectiveness coefficient for concrete confined by steel is usually taken between 2.8 and 4.1. Campione and Miraglia (2003) found that the above values overestimate the confinement effectiveness coefficient for concrete wrapped with FRP and some other confining material. They found the confinement effectiveness coefficient for FRP wrapped concrete to be 2. For the purpose of this study the confinement effectiveness coefficient was taken as 2.

The axial strain of confined concrete at the peak stress (ε_{co}) was determined in a similar manner as unconfined concrete using the following expression (MacGregor 1997):

$$\varepsilon_{co} = 1.8 \cdot \frac{f''_{cc}}{E_c} \quad (6)$$

Equations (5) and (6) were combined with the modified Hognestad stress-strain equation as follows:

$$f_c = f''_{cc} \cdot \left[\frac{2 \cdot \varepsilon_c}{\varepsilon_{co}} - \left(\frac{\varepsilon_c}{\varepsilon_{co}}\right)^2\right] \quad (7)$$

$$f_c = f''_{cc} \cdot [1 - D_c \cdot (\varepsilon_c - \varepsilon_{co})] \quad (8)$$

Where ε_c is the concrete strain, ε_o is the strain at peak stress of unconfined concrete and ε_{cu} is the ultimate strain. The modified Hognestad equations model the ascending branch (AB) with a parabolic relationship and the descending branch BC with a linearly descending curve. The equation for region UC is based on the deterioration constant (D_c) that controls the slope of the line.

$$f_c = f''_{cc} \cdot \left[\left[\frac{2 \cdot \varepsilon_c}{\varepsilon_{co}} - \left(\frac{\varepsilon_c}{\varepsilon_{co}}\right)^2\right] \cdot H(\varepsilon_{co}) + [1 - D_c \cdot (\varepsilon_c - \varepsilon_{co})] \cdot H(\varepsilon_{co} - \varepsilon_c)\right] \quad (9)$$

The material properties of the UG ribs were used to construct the stress-strain curve of the UG confined concrete. The average strength of the control cylinders tested in displacement control mode was taken as the strength of unconfined concrete (f'c). An average UG sheets diameter of 200 mm was used. The ultimate concrete strain ε_{cu} was assumed to be 15000 micro strains. The average stress-strain curve for the BG confined concrete was constructed using data from all tested columns. The average stress-strain curve for the unconfined cylinders was also constructed for comparison. The deterioration constant was taken equal to 40 for 1 layer UG confined concrete columns, and 7 for 2 layers confined concrete columns, to match post peak experimental data. All

three curves are depicted in Figure 16 and Figure 16. The modified Hognestad matches well with the experimental curve.

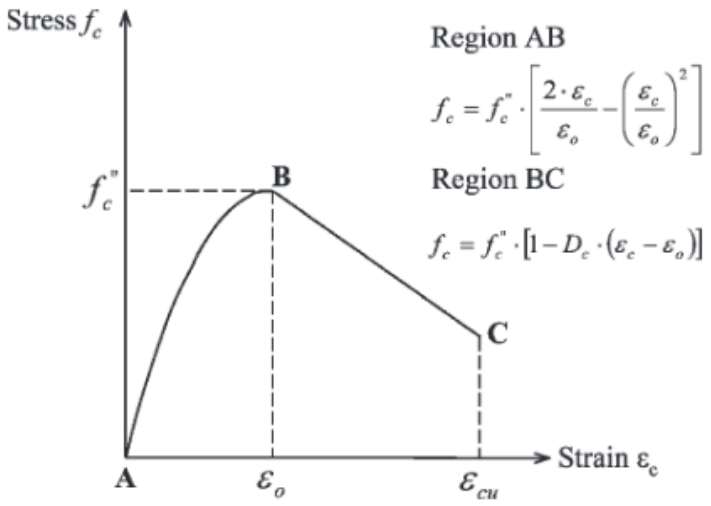

Figure 52 Modified Hognestad Stress Strain-Curve; Park and Pauly

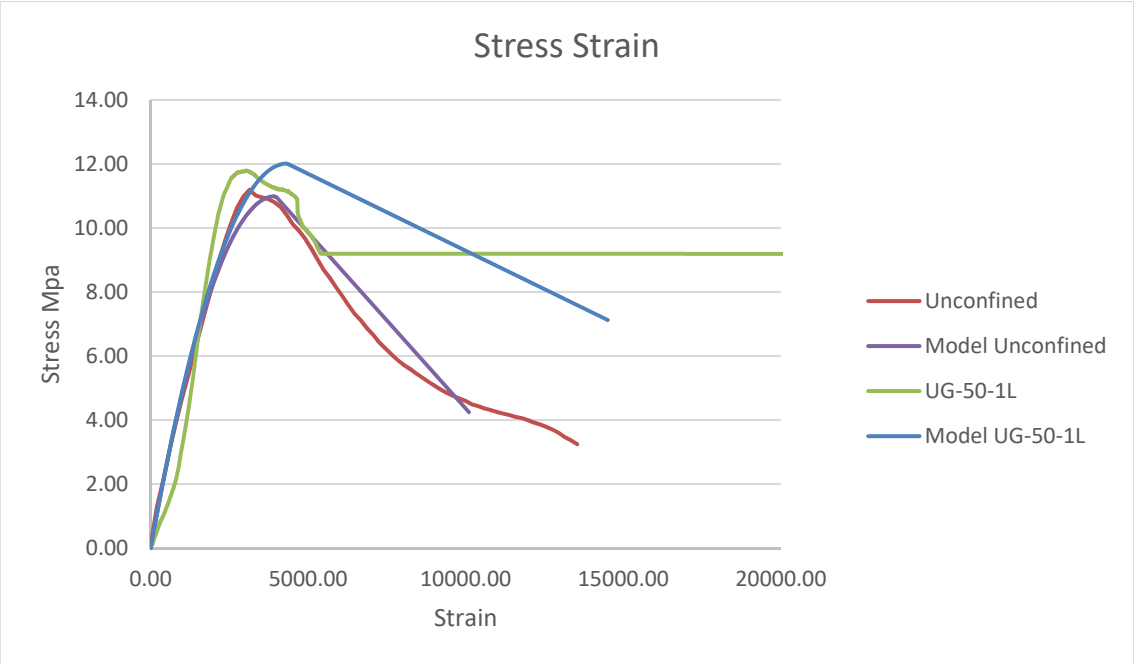

Figure 53 Experimental and Modified Hognestad Model stress-strain curves of unconfined and 1-layer UG confined specimens

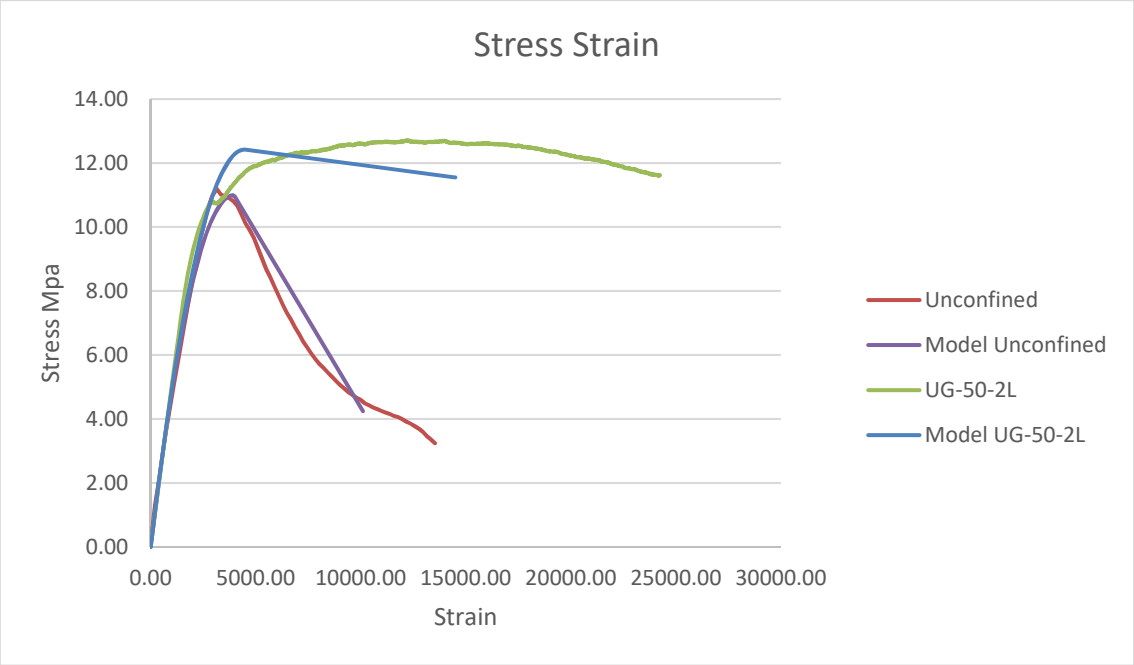

Figure 54Experimental and Modified Hognestad Model stress-strain curves of unconfined and 2-layer UG confined specimens

CHAPTER VI

CONCLUSIONS

The following conclusions can be drawn based on the experimental and analytical research investigation presented in this thesis:

1. Columns confined with Geogrids can develop ductile behavior under simulated monotonic loading. The use of Geogrids sheets as confinement reinforcement substantially increases deformability of the columns.
2. Inelastic column behavior obtained in Geogrids columns are comparable to those obtained with conventional reinforcement.
3. Geogrids provide effective confinement to the core column section, similar to the conventional steel reinforcement concrete column.
4. The strain data recorded during column tests indicate that the strength of Geogrids could be mobilized to a large extent, developing strains of 20000 Macrostrains to 30000 Macrostrains in most columns with a maximum value of 35000 Macrostrains. The recommended strain value for use in design is 20000 Macrostrains, which reflects a representative value for most columns.
5. The analytical model developed for the stress-strain relationship of concrete with internally Geogrids confined concrete provides good agreement with experimental data.
6. The confinement model proposed by Modified Hognestad Stress Strain-Curve can be applied to Geogrids confined concrete columns with

appropriate modifications introduced to strength of both type of geogrids.

REFERENCES

Abdesssemed, M., Kenai, S., & Bali, A. (2015a). Experimental and numerical analysis of the behavior of an airport pavement reinforced by geogrids. Construction and Building Materials, 94, 547-554.

Abdesssemed, M., Kenai, S., & Bali, A. (2015b). Experimental and numerical analysis of the behavior of an airport pavement reinforced by geogrids. *Construction and Building Materials, 94*, 547-554.

ACI committee 440 on FRP composites - update. (2000, Aug 21,). *Advanced Materials & Composites News*

ADINA R&D, I. (2012). *Theory and modeling guide volume I: ADINA*. Watertown, MA:

Al-Hedad, A. S. A., Bambridge, E., & Hadi, M. N. S. (2017). Influence of geogrid on the drying shrinkage performance of concrete pavements. *Construction and Building Materials, 146*, 165-174.

Article Scientific research, & essays · November 2010.*Reinforced pavement above trench under urban traffic load: Case study and finite element (FE) analysis*

Chehab, G. R., & El Meski, F. (2014). Flexural behavior of concrete beams reinforced with different types of geogrids. *Journal of Materials in Civil Engineering, 26*(8), 4014038. 10.1061/(ASCE)MT.1943-5533.0000920

Chidambaram, R. S., & Agarwal, P. (2016). Performance evaluation of geogrid-confined beam-column joints with steel fiber reinforced concrete under cyclic loading. *Journal of Testing and Evaluation, 44*(1), 582-598.

Demir, A., Yildiz, A., Laman, M., & Ornek, M. (2014). Experimental and numerical analyses of circular footing on geogrid-reinforced granular fill underlain by soft clay. *Acta Geotechnica, 9*(4), 711-723.

Itani, H., Saad, G., & Chehab, G. (2016). The use of geogrid reinforcement for enhancing the performance of concrete overlays: An experimental and numerical assessment. *Construction and Building Materials, 124*, 826-837.

Khodaii, A., Fallah, S., & Moghadas Nejad, F. (2009). Effects of geosynthetics on reduction of reflection cracking in asphalt overlays. *Geotextiles and Geomembranes, 27*(1), 1-8.

Lam, L., & Teng, J. G. (2004). Ultimate condition of fiber reinforced polymer-confined concrete. *Journal of Composites for Construction, 8*(6), 539-548. 6(539)

Lam, L., & Teng, J. G. (2003). Design-oriented stress–strain model for FRP-confined concrete. *Construction and Building Materials, 17*(6), 471-489.

Lee, S., & Won, J. (2014). Flexural behavior of precast reinforced concrete composite members reinforced with structural nano-synthetic and steel fibers. *Composite Structures, 118*, 571-579.

Liu, Z., & Ling, H. I. (2001). Performance of geosynthetic-reinforced asphalt pavements. *Journal of Geotechnical and Geoenvironmental Engineering, 127*(2), 177-184. 2(177)

MacGregor, J. G. 1. (1997). *Reinforced concrete : Mechanics and design*. United States:

Mander, J. B., Priestley, M. J. N., & Park, R. (1988). Theoretical stress-strain model for confined concrete. *Journal of Structural Engineering, 114*(8), 1804-1826. 8(1804)

Michels, J., Waldmann, D., Maas, S., & Zürbes, A. (2012). Steel fibers as only reinforcement for flat slab construction – experimental investigation and design. *Construction and Building Materials, 26*(1), 145-155.

Norambuena-Contreras, J., & Gonzalez-Torre, I. (2015). Influence of geosynthetic type on retarding cracking in asphalt pavements. *Construction and Building Materials,*

Park, R., & Paulay, T. (1975). *Reinforced concrete structures*. New York: Wiley.

Park, Y., Abolmaali, A., Mohammadagha, M., & Lee, S. (2015). Structural performance of dry-cast rubberized concrete pipes with steel and synthetic fibers. *Construction and Building Materials, 77*, 218-226. 10.1016/j.conbuildmat.2014.12.061

Pessiki S, P. A. (1997). Axial load behavior of large scale spirally-reinforced high-strength concrete columns. *Aci Structural Journal,* (94(3)), 304–314.

Pujadas, P., Blanco, A., Cavalaro, S., & Aguado, A. (2014). Plastic fibres as the only reinforcement for flat suspended slabs: Experimental investigation and numerical simulation. *Construction and Building Materials, 57*, 92-104.

Rossini, G., Bevilacqua-Aldobrandini, G., & Müller, R. (2012). *Adina*. Leipzig: Leipziger Univ.-Verl.

Siva Chidambaram, R., & Agarwal, P. (2014). The confining effect of geo-grid on the mechanical properties of concrete specimens with steel fiber under compression and flexure. *Construction and Building Materials, 71*, 628-637.

Siva Chidambaram, R., & Agarwal, P. (2015). Flexural and shear behavior of geo-grid confined RC beams with steel fiber reinforced concrete. *Construction and Building Materials, 78*, 271-280.

Sivakamasundari, S., Daniel, A. J., & Kumar, A. (2017). Study on flexural behavior of steel fiber RC beams confined with biaxial geo-grid. *Procedia Engineering, 173*, 1431-1438.

Teng, J. G., & Lam, L. (2004). Behavior and modeling of fiber reinforced polymer-confined concrete. *Journal of Structural Engineering, 130*(11), 1713-1723.

X. Tang, G.R. Chehab, & S. Kim. (2008). *Laboratory study of geogrid reinforcement in portland cement concrete*

Yalciner, H., Kumbasaroglu, A., Ertuc, İ, & Turan, A. İ. (2018). Confinement effect of geo-grid and conventional shear reinforcement bars subjected to corrosion. *Structures, 13*, 139-152. 10.1016/j.istruc.2017.12.004

Yetimoglu, T., Wu, J. T. H., & Saglamer, A. (1994). Bearing capacity of rectangular footings on geogrid-reinforced sand. *Journal of Geotechnical Engineering, 120*(12), 2083-2099. 12(2083)